Thermodynamic and spectroscopic studies of Cd^{2+} binding to the regulatory domain and full length human cardiac troponin C (HcTnC): Elucidating plausible Cd^{2+} binding sites

by

Lindsay Michelle Fulcher

July, 2015

Director of Thesis: Anne M. Spuches

Major Department: Chemistry

Abstract

Toxic metals such as cadmium (Cd^{2+}) have been shown to bind to and interfere with various calcium (Ca^{2+}) binding proteins including the regulatory protein cardiac troponin C (cTnC). Recent structural data has shown that Cd^{2+} binds to both EF hand Ca^{2+} binding loops in the regulatory N-domain of human cTnC including EF hand loop I, which normally does not bind metal. Although the data reveal two Cd^{2+} ions bound to the protein, the binding constants and other thermodynamic parameters are not known. Therefore, the goal of this research project is to use Isothermal Titration Calorimetry (ITC) to obtain thermodynamic parameters such as K, ΔH, ΔG and ΔS of Cd^{2+} binding to both the full length and N-domain (amino acid residues 1-89) of HcTnC and compare the parameters to our previous data with Ca^{2+}. Through our results we hope to shed light on potential mechanisms of cadmium toxicity.

Thermodynamic and spectroscopic studies of Cd^{2+} binding to the regulatory domain and full length human cardiac troponin C (HcTnC): Elucidating plausible Cd^{2+} binding sites

A Thesis

Presented To the Faculty of the Department of Chemistry

East Carolina University

In Partial Fulfillment of the Requirements for the Degree

Masters of Science Degree in Chemistry

by

Lindsay Michelle Fulcher

July, 2015

Thermodynamic and spectroscopic studies of Cd^{2+} binding to the regulatory domain and full length human cardiac troponin C (HcTnC): Elucidating plausible Cd^{2+} binding sites

by

Lindsay Michelle Fulcher

APPROVED BY:

DIRECTOR OF
THESIS: _____
Anne M. Spuches, PhD

COMMITTEE MEMBER: _____
Colin Burns, PhD

COMMITTEE MEMBER: _____
Yumin Li, PhD

COMMITTEE MEMBER: _____
Joseph Chalovich, PhD

CHAIR OF THE DEPARTMENT
OF CHEMISTRY: _____
Andrew Morehead, PhD

DEAN OF THE
GRADUATE SCHOOL: _____
Paul J. Gemperline, PhD

Acknowledgments

I would like to thank my thesis advisor Dr. Anne M. Spuches, for her incredible motivation, determination and sincere confidence in my abilities to finish my thesis. Her constant support and encouragement helped me to keep going even during the toughest of times. I would also like to thank Dr. Joseph Chalovich (Department of Biochemistry and Molecular Biology at the Brody School of Medicine) and Dr. Paul Hager (Department of Biology at ECU) for all of their support and aid in establishing the methods for protein purification. In addition, I would like to thank the other members of my thesis committee, Dr. Andrew Morehead, Dr. Colin Burns, and Dr. Yumin Li for their support in helping me succeed throughout my graduate education. Last but not least, I would like to thank my family and friends for their constant support and endless confidence in my ability to succeed. Everyone before mentioned has been paramount to my success and completion of the program and I will be forever grateful for all you have done for me during this time in my life.

Table of Contents

List of Tables

List of Figures

List of Abbreviations

HSAB: Hard Soft Acid Base theory

TnC: Troponin C Subunit

cTnC: Cardiac Troponin C

HcTnC: Human Cardia Troponin C

EFβS: EF-Hand β-Scaffold

ATP: Adenosine Triphosphate

ADP: Adenosine Diphosphate

Pi: Phosphate ion

Tm: Tropomyosin

Tn: Troponin

TnT: Troponin T Subunit

TnI: Troponin I Subunit

TnT1: N-terminus region of Troponin T

TnT2: C-terminus region of Troponin T

cTnI: Cardiac Troponin I

sTnC: Skeletal Troponin C

FHC: Familial Hypertrophic Cardiomyopathy

FDA: Food and Drug Administration

ITC: Isothermal Titration Calorimetry

***n*:** Stoichiometric Ratio

K_b: Binding constant

ΔH: Change in Enthalpy

ΔG: Change in Gibb's Free Energy

ΔS: Change in Entropy

K_{eq}: Equilibrium Constant

ΔC_p: Change in Heat capacity

HcTnC: Human Cardiac Troponin C

$HcTnC_{1\text{-}89}$: Truncated form of Human Cardiac Troponin C including amino acids 1-89

EDTA: Ethylenediamminetetraacetic Acid

DMSO: Dimethyl sulfoxide

MES: 2-(N-morpholino)ethanesulfonic Acid

Bis-Tris: 2-Bis(2-hydroxyethyl)amino-2-(hydroxymethyl)-1,3-propanediol

Chapter 1: Introduction

1.1 Chemical Properties of Cadmium

Cadmium is a member of the Group 12 transition elements of the Periodic Table (Z = 48, atomic mass 112.41 g/mol) and therefore contains a stable d^{10} electron configuration ($[Kr]4d^{10}5s^2$). It can exist in the +1 (Cd^+) oxidation state but the closed d-shell stabilization causes cadmium to almost exclusively be found in the +2 (Cd^{2+}) oxidation state in the natural environment [1]. Cadmium is found in the earth's crust with a concentration in the lithosphere of 0.08–0.1 ppm, which is roughly 650 fold lower than its Group 12 neighbor, Zinc [2,3], and is characterized by its relatively low melting (321 °C) and boiling (767 °C) points and a density equal to 8.65 g/cm^3 at 20 °C [1,4].

Cadmium is most abundantly found as CdS in the crystal lattice of various ores, mainly those involving Zinc [3]. This common occurrence is due to the Hard Soft Acid Base (HSAB) properties of cadmium. The HSAB theory defines hard acid and hard base ions as those that possess small atomic/ionic radii, high oxidation states, and low polarizability, while exclusively hard bases possess a high electronegativity [5]. Soft acids and soft bases, on the other hand, tend to have large atomic/ionic radii, low or zero oxidation states, and high polarizability, while low electronegativity is an additional trait of soft bases. Furthermore, soft acids tend to form stable covalent bonds with soft bases while hard acid ions tend to form ionic bonds with hard base anions. As a soft Lewis acid, the Cd^{2+} ion prefers to interact with soft ligand bases, such as sulfur, resulting in a very stable structure. The stable interaction between cadmium and sulfur make zinc ores such as sphalerite, (Zn/Fe)S, a prime source for cadmium [6,7].

Cadmium-sulfide salts can be extracted as by-products from the refinement process of zinc ore bodies. Once isolated, these salts are collected and further used as additives in various commercial products. For example, cadmium sulfide, the most common salt, forms a stable crystal lattice that produces a yellow hue when subjected to light. Therefore, this salt is used as a yellow pigment and serves as a popular additive in various paints and coloring materials [7,8]. Cadmium sulfide can also serve as a p-type semiconductor by coupling with a doped semiconductor to produce photovoltaic cells for solar panels [9].

Cadmium can also be found in complex with other elements, such as selenium. CdSe salts is another example of a stable cadmium complex that has a wide variety of uses. Similar to cadmium sulfide, CdSe is often used as a color additive due to its red pigment, commonly known as *cadmium red*. To painters who work with pigment based paints, cadmium yellows, oranges, and reds are the most brilliant and long-lasting colors to use [10]. Cadmium's versatile role makes it a very viable material for the production of pigments, color plastics, inks, paints, rubber, and other consumer goods. It also serves as a major source for metal plating, the production of NiCd batteries, and as a neutron absorber in nuclear reactors [11].

1.2 Cadmium Mobilization and Exposure

Cadmium is mobilized in the environment naturally through processes such as volcanic eruptions, physical and chemical weathering of parent rock material or derived soils, burning of vegetation, sea salt spray, and the production of marine biogenic aerosols [12-15]. Cd^{2+} is additionally mobilized through human activities, such as the processing of zinc ores, combustion of fossil fuels, manufacturing and usage of cadmium containing products, and incineration of the former waste. From the 1930's to 1990, cadmium production rose from ~20 tons/ year and

stabilized at ~20,000 tons / year [16]. This increase is most likely attributed to cadmiums many uses in today's consumer products such as NiCd batteries, pigments, and plastic stabilizers [17]. These anthropogenic sources account for the majority of cadmium emitted into the environment [16].

This increase in environmental exposure has led to accumulated levels of cadmium in air, water and food sources, thereby enabling numerous routes in which humans can be exposed to this metal. It is estimated that workers in certain occupations, such as the mining and farming industries, are exposed to cadmium at significantly higher levels than the general public [18]. Similarly, people living in areas contaminated with cadmium are exposed to higher amounts of the metal. Other sources of human exposure to cadmium include diet and cigarette smoke due to the high accumulation in various plants, particularly tobacco, and a variety of food sources.

The average person in the US consumes approximately 30 µg of cadmium per day through food sources [18]. However, this value may increase or decrease depending on the types of food an individual includes in their diet. For example, certain food categories are considered to have higher levels of cadmium, such as rice, soybeans, peanuts, bivalve mollusks, and oysters [19,20]. In Pacific oysters, cadmium levels are found to be 13.5 mg/kg dry weight while an even higher cadmium content was reported for some New Zealand Bluff oysters [21]. Oilseeds, such as sunflower seeds, peanuts, and flaxseeds, are shown to accumulate cadmium from the soil at levels ranging from 0.2 to 2.5 mg/kg. High cadmium levels (7-76 mg/kg wet weight) were also found in the offal of dugongs (marine mammals similar to manatees) and turtles [22].

Exposure to cigarette smoke is another major source of cadmium exposure. Tobacco plants selectively accumulate cadmium in the form of Cd^{2+} ions from the soil and typically contain 1-2 µg of cadmium/g dry weight [23]. This amounts to 0.5-1 µg of cadmium per

cigarette. 10% of inhaled cigarette smoke is deposited in the lungs while 30-40% of the inhaled smoke is absorbed into the systemic blood circulation [23]. Therefore, smokers are found to have 4-5 times higher cadmium blood levels and 2-3 times more cadmium in their kidneys [23].
The main routes of cadmium absorption in the body are through the gastrointestinal tract and lungs. An average individual ingests between 30-50 µg/day [23] of cadmium thus absorbing between 1 and 10% [24]. The intestine normally absorbs 6% of total ingested cadmium [23,24]. However individuals with low iron or essential metal deficiency are reported to absorb an average of 9% ingested cadmium. In addition, the lungs, have been reported as the major route of cadmium adsorption with the average person absorbing 50% of inhaled cadmium through this route [25]. The skin is not a prominent route of absorption but it is also known to intake a small percentage (~0.5%) of cadmium upon exposure [23].

1.3 Cadmium Toxicity

Although cadmium may be useful in the production of various materials, it does not serve a biological role in maintaining the function and regulation of cellular life in the cellular tissues of higher ordered species. This metal is considered toxic, because when absorbed, Cd^{2+} can interact strongly through covalent bonds with the sulfur atoms of various protein ligands leading to unintentional inhibition or activation of biological pathways. For example when cadmium is absorbed by tissue cells, cadmium can act as a catalyst in forming reactive oxygen species, increase lipid peroxidation, and decrease circulating antioxidants, by interacting with glutathione and protein-bound sulfhydryl groups [26]. In humans, such interactions are known to interfere with the cellular function and regulation in the tissues of the kidney, liver, and heart. As a result,

chronic exposure and constant accumulation of cadmium at these sites has been contributed to the onset of severe health issues in these specific tissues [12,27].

Previous studies have demonstrated that certain health complications in the kidneys, liver, or heart, arise when cadmium accumulates to specific concentrations at these target tissue sites. For example, cardiovascular effects have been reported at cellular levels as low as 0.1μM Cd^{2+} concentration [28] while urinary Cd^{2+} levels greater than 0.88 μg/g creatinine are shown to increase the risk of myocardial infarction in women [29]. Additionally, glomerular impairment has been reported at urinary cadmium levels of 0.8 μg/g creatinine [30]. Furthermore, sustained blood and urine levels in a range of 25-50 μg/L or 25-75 μg/g creatinine, respectively, have been shown to induce renal failure in patients chronically exposed to cadmium metal. Reportable creatine levels higher than those previously discussed, has been associated with death, mostly as result of complete renal dysfunction [31]. Although these values may seem small, they are obtainable when considering the typical dietary intake of cadmium is about 30-50 micrograms of cadmium per day (μg/day) [18].

Cadmium exposure is a concern to human health considering the toxic effects induced by the metal at such low concentrations. The effects of cadmium toxicity on cardiovascular disease (CVD) is of particular interest in the research field, considering CVD is the number one killer of American males and females [31]. In 2004 an estimated 17.1 million people died due to CVDs and this number will further increase to an estimated 23.6 million by 2030[31]. Hypertension, and hypercholesterolemia, constitute about 50–75% of all CVDs, while 25-50% of causes for CVD still remains unknown. Although there is still an urgent need to search for and define new CVD risk factors, recent studies have provided promising results in pursuit of identifying possible mechanisms of cadmium toxicity on CVD [31].

A recent crystal structure (Figure 1C), has demonstrated that cadmium can bind to the N-terminal regulatory domain of cardiac Troponin C (cTnC) [32,33], a regulatory protein responsible for maintaining muscle contraction in the heart [34]. This protein contains two calcium binding EF hand motifs in the N-domain, defined as EF hand loop II, or the calcium binding loop, and EF hand loop I, which is a vestigial site and does not bind calcium, see Figure 1B [34]. The study shows that when cTnC is subjected to cadmium, Cd^{2+} metal ions not only interact in both EF hand loops at the N-terminus of the protein, but the binding of this metal induces a slight structural transition in the protein that differs from that observed when calcium binds to the N-domain of cTnC [32]. Cadmium binding to either EF hand I or II may adversely alter the function of the protein.

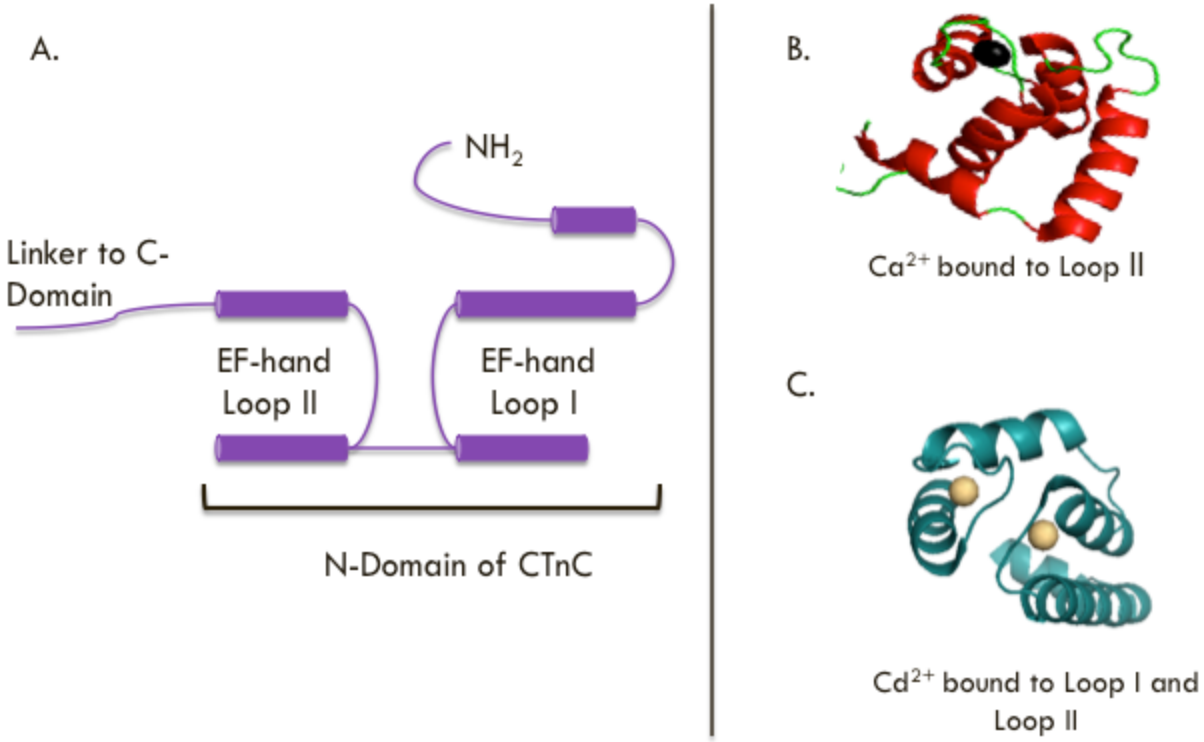

Figure 1. (A) The EF hand loops I and II in the N domain of cTnC. (B) Ca^{2+} binds to EF hand loop II but not EF hand loop I [35]. (C) Crystal structure demonstrates that in the presence of Cd^{2+} both EF hand sites bind Cd^{2+} metal [32,33].

Although one can speculate that the presence of Cd^{2+} in cardiac cells can disrupt protein function and hence muscle regulation, by interacting with the regulatory N domain of cTnC, there is not enough information to deduce a mechanism for the effects of cadmium toxicity on CVD. Further experimental investigation is needed to determine if cadmium binding to cTnC effects the calcium affinity for the protein, and in turn, effects the function of cTnC.

1.3.1 Fate and Transport of Cadmium in the Cell

Cadmium is absorbed in the body and taken up in the liver as the Cd^{2+} ion where it forms complexes with small peptides and proteins via sulfhydryl groups, including glutathione (GSH) or the high affinity metal binding protein metallothionein (MT) [36]. Cd^{2+} has been shown to bind to metalloproteins with high affinity, evident by the apparent stability constants for MT and GSH of ~10^{-25}–10^{-14} M^{-1} and ~10^{-9} M^{-1}, respectively[37,38]. This high affinity binding enables the displacement of essential metals from these proteins by ligand exchange [39-41] which may result in inhibition of their function. However, once bound to the protein, Cd^{2+} complexes such as Cd^{2+}-GSH or $(Cd^{2+})_7$-MT are then either secreted into the bile or released into circulation [27] where they are rapidly transported by the blood to different organs in the body. These complexes can then exchange Cd^{2+} with cellular membrane bound transporter proteins or be taken up by cells via receptor-mediated endocytosis [42].

Cd^{2+} uptake is most commonly known to occur through facilitated diffusion and active transport via membrane bound ion channels and solute carriers. However, since Cd^{2+} is considered non-essential in humans, cells lack specific entry sites for this toxic metal. Therefore, Cd^{2+} is able to move to the interior of the cell by binding to transport membrane proteins that are specific to essential metals. Cd^{2+} can also enter cells by following the massive fluxes of other cations, which can be triggered by changing conditions, especially for excitable cells, via channels with leaky selectivity filters [43].

Another proposed pathway for Cd^{2+} uptake in cells is through receptor-mediated endocytosis. This occurs when Cd^{2+} is in complex with low molecular weight thiols, such as glutathione (GSH) or cysteine (Cys), which serve as molecular homologs. These complexes can

enter cells through organic transporter sites by mimicking amino acids, oligopeptides, or organic cations [7].

Once inside the cell, Cd^{2+} can impose multiple effects on cellular functions including cell-cycle progression, DNA replication and repair, differentiation, and apoptotic pathways [44]. Specifically, $(Cd^{2+})_7$-MT complexes, are analogous to endogenous biological molecules [41]. This "molecular mimicry" enables the transport of Cd^{2+} to cellular tissues if those target cells possess transport pathways for essential metals or biological molecules [41]. Therefore, organs which utilize essential metals for various functional purposes, such as the liver, kidney, testis, spleen, heart, lungs, thymus, salivary glands, epididymis, and prostate, serve as major cadmium storage sites [26,45].

After Cd^{2+} moves into cells, its estimated half-life in various tissues is 10 years or greater [46,47]. This long half-life is in part due to the affinity of the metal with intercellular transport biomolecules and metal binding proteins. Transport biomolecules located on the interior of a cell are known to have a stronger affinity for cadmium when compared with the affinity of this metal to exterior membrane proteins. Due to these strong interactions, Cd^{2+} is prevented from diffusing out of the cell, thereby accumulating in tissues overtime. Also, the ability of Cd^{2+} to interact with intracellular protein sites can greatly affect the overall processes involved in the cell. This imposes a great threat to the lifespan of certain cells and tissues, and ultimately, the overall health and quality of life for a specific individual.

1.4 Cd^{2+} Interactions with Proteins

According to "Hard Soft Acid Base Theory" (HSAB), Cd^{2+}, a soft metal ion, prefers to interact with soft base ions such as sulfur. Previous research has focused on the covalent thiolate

bond formed between Cd^{2+} and the cysteine residues of a variety of proteins [48]. As mentioned above, much work has been done to elucidate Cd^{2+} to cysteine residues present within metallothioneins and other transporter proteins [36]. Metallothioneins have been reported to play a detoxification role and are upregulated under heavy metal stress [36].

Cadmium ions have been shown to coordinate to the metal binding sites of carbonic anhydrase and horse liver alcohol dehydrogenase through means of two cysteines and one histidine residue [49,50]. Although Cd^{2+} is the native cofactor of carbonic anhydrase of the marine algae *Thalassiosira weissflogi* [51], the interaction of this metal within mammalian metal binding proteins is non-essential and thus considered to be a toxic interaction [52]. More recently, Cd^{2+} has been shown to form a thiolate bond with the sulfur atom of the cysteine residue in the EF hand 1 site of Ca^{2+} binding protein, human cardiac TnC (HcTnC) [33].

In addition to cysteine residues, Cd^{2+} has been found to coordinate with a very high affinity to oxygen rich metal binding sites. In particular, Cd^{2+} can bind to EF hand proteins that are specific for Ca^{2+} with a similar geometry and coordination number as Ca^{2+}. Although Cd^{2+} and Ca^{2+} differ in their HSAB properties and oxygen is considered a hard base, both calcium and cadmium have similar ionic radii and size to charge ratios. The ionic radii for Ca^{2+} and Cd^{2+} are 0.99 Å and 0.97 Å respectively [53] while the charge/size ratios reported for Ca^{2+} and Cd^{2+} were 2.02 e/Å and 2.06 e/Å, respectively [53].

Due to the similarities listed above, Cd^{2+} has often been used as an effective substitute and probe for many Ca^{2+} binding proteins [52,54]. An isotope of cadmium, ^{113}Cd, is often used in the NMR analysis of calcium binding proteins [55,56,56-59]. Several crystal structures of EF hand proteins bound to Cd^{2+} have been reported: parvalbumin [60], calpain [61], sTnC [57], and cardiac troponin C (cTnC) [32]. The primary coordination spheres of Cd^{2+} in these proteins were

compared to their Ca^{2+} counterparts and all were shown to adopt the pentagonal bipyramidal geometry, except for EF I in cardiac troponin C [32]. Since Cd^{2+} can replace Ca^{2+} in proteins without disrupting the protein structure, many EF hand proteins have been shown to be activated by Cd^{2+} including CaM, Calbindin D9K, and skeletal troponin C (sTnC) [56,62,63].

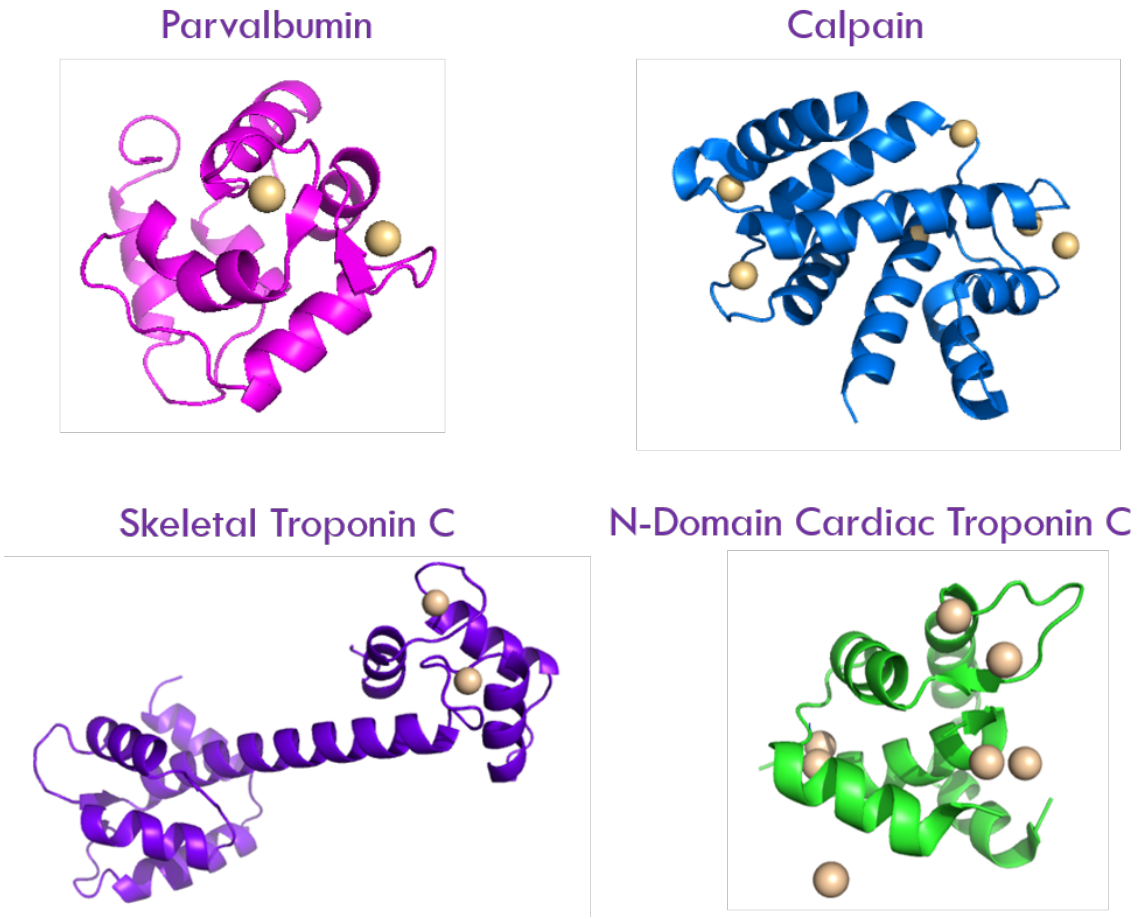

Figure 2. Interactions between Cd^{2+} and the calcium binding sites of parvalbumin [60], calpain [61], C-domain sTnC [57], and the EF I (functional, calcium site) and EF II (vestigial site) in the N terminal domain of cTnC [32]. Cd^{2+} coordinates in each of these sites, except for EF I, and EF II of cTNC in pentagonal bipyramidal geometry. A distorted pentagonal bipyramidal geometry and a distorted octahedral geometry is observed for the coordination of Cd^{2+} in sites EF II and EF I of N-cTnC, respectively.

1.5 EF Hand Proteins

In order to understand how Cd^{2+} may activate or alter the function of EF hand proteins, it is important to first understand the role Ca^{2+} ions plays in the chemistry of these proteins. Ca^{2+} serves as an important intracellular signaling ion in biological systems and is used in a variety of intracellular signaling pathways such as fertilization, cell differentiation, muscle contraction, and apoptosis [54]. Intracellular "free" Ca^{2+} ion concentrations range from 10 to 100 nM while extracellular concentrations are found to be ~ 1.2 mM [64]. This gradient helps facilitate Ca^{2+} entry into cellular cytoplasmic space thus elevating intracellular calcium concentration to a range of 1 to 100 μM [64].

Since Ca^{2+} is an important ion to biological systems with diverse functions, calcium concentrations are tightly regulated both intracellularly and extracellularly. Once Ca^{2+} flows into the cytoplasm of a cell it becomes bound to a wide variety of calcium binding proteins (CaBP). Many of these CaBP's belong to a homologous family that bind this metal cation using a characteristic helix-loop-helix structural motif, termed the EF hand [65]. These proteins can bind to the Ca^{2+} ion with association constants ranging from 10^5 M^{-1} to well above 10^{10} M^{-1} [64]

The EF hand motif was first discovered in 1973 when Kretsinger and coworkers [66] showed calcium bound in a distinct E-helix-loop-F-helix structure of the crystallized protein parvalbumin. This discovery gave rise to the EF hand Ca^{2+} binding motif which has now been identified in over 3000 proteins, all of which share homologous structures. The EF-hand motif is among the most common in animal cells [67] and more than 1000 have been identified from their unique amino acid sequences. The turn–loop structure provides the bulk of the ligands for the bound cation [65].

These motifs are usually organized into structural units/domains containing two or more EF hands that form highly stable helical bundle [68]. Because of its specificity for Ca^{2+}, this motif is a key component of various proteins in calcium signaling pathways and, not surprisingly, has been evolutionarily conserved.

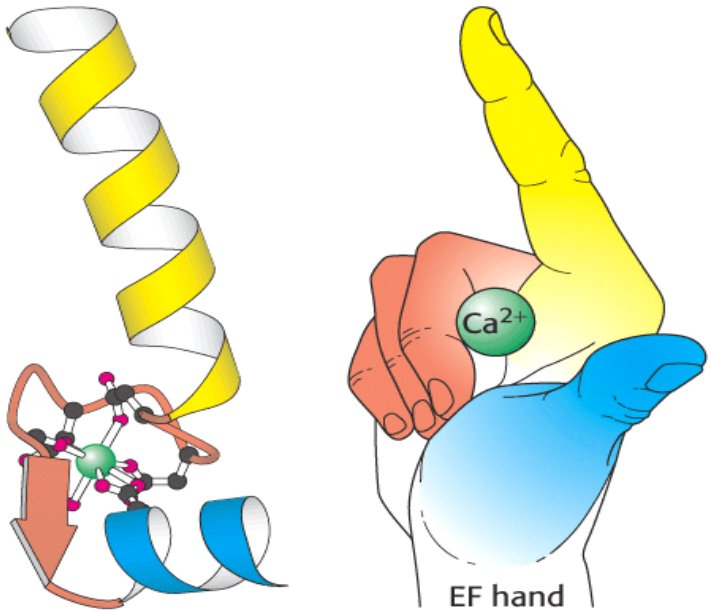

Figure 3. A representation of the E-helix-loop-F-helix structure that constitutes the EF hand motif. Calcium ion coordinate with the ligands available in the loop region of the EF hand structure [69].

1.5.1 Classes of EF Hand Proteins

The EF hand is thought to have originally developed from a common precursor domain. It is believed that small variations between EF hand proteins are a result of successive gene duplication and deletion. These differences in sequences and structures allow EF-hand proteins

to perform a diverse range of functions. There are two primary classes of EF-hand proteins: Ca^{2+} buffer and Ca^{2+} sensors.

The first category of EF hand proteins are known as Ca^{2+} signal modulators, or Ca^{2+} buffers. These proteins modulate the duration of Ca^{2+} signals and help maintain Ca homeostasis within a cell [70]. They do so by temporarily binding free Ca^{2+} ions in order to transmit the signal throughout the cell, or to remove the metal from the cell [65]. Since these proteins do not interact with target sites like sensors proteins, these calcium binding molecules are considered to interact with calcium for structural purposes. Because of this, EF hand buffers are usually found at higher concentrations in a cell and usually demonstrate higher affinities for calcium than sensor proteins. Also, the interaction between calcium and the EF hand sites of buffering proteins induces a significantly smaller conformational change in the protein when compared to the structural changes observed when calcium binds to sensor proteins [65]. Examples of buffer proteins are parvalbumin, calretinin, and calbindin [65].

The second class of EF hand proteins include the Ca^{2+} sensors. These are proteins or molecules that bind Ca^{2+} as a result of an increase in concentration of calcium. Protein sensors respond to this signal by interacting with the metal ion, which in turn, induces a structural change throughout the protein, thereby exposing binding sites for target proteins to interact. This interaction causes a structural change in the protein, which further facilitates subsequent interactions with other molecular components in the cell. By means of this interactive cascade of events, diverse biochemical responses are induced, and the original signal is ultimately translated from cell to cell [65]. Examples of Ca^{2+} sensors are CaM, recoverin, myosin light chain proteins, s100 proteins, and TnC [66].

The binding of Ca^{2+} to sensor proteins is accompanied by conformational changes within the protein. For example, the inter-helical changes within the amino and carboxy-terminal EF hand domains of CAM [71-73] and the amino-terminal domains of skeletal muscle TnC are shown to change 60° upon Ca^{2+} binding [66]. This conformational change is considered large when compared to the inter-helical movements of EF hand helices in Ca^{2+} buffering proteins such as calbindin D9K and recoverin [66]. The angles observed in EF hand domains of these buffering proteins are shown to deviate from each other at an angle of 12° or less [74].

Protein domains showing large conformational changes are known to have a trigger function in the activation of target proteins and therefore can be termed regulatory domains [66]. Also, as part of their regulatory role, these proteins are shown to contain EF hand sites that have a lower affinity for calcium when compared to that of buffering proteins. The selective nature of these proteins for metal ions is characteristic of their role as regulatory molecular units in biological pathways.

Table 1: A description of the different classes of EF hand Ca^{2+} binding proteins, Ca^{2+} buffers and Ca^{2+} sensors, and their respective differences.

EF hand Class	Function	Binding Affinity	Induced conformational change	Examples
Ca^{2+} Buffers	Interact with Ca^{2+} for structural purposes	High affinity for Ca^{2+}	Small	Parvalbumin, Calretinin, and Calbindin
Ca^{2+} Sensors	Interact with calcium for regulatory purposes	Low affinity for Ca^{2+}	Large	CaM, Recoverin, Myosin light chain proteins, s100 proteins, and TnC

1.5.2 Calcium Binding Loop of EF Hand

The EF hand loop is commonly referred to as positions 1-12 where amino acids located at positions 1, 3, 5, 7, 9, and 12 participate in chelating Ca^{2+} ion. The chelating residues of the loop are defined based on their position during calcium coordination and sometimes arrange themselves in a linear position, while others take on a tertiary geometry, imposed by their alignment on the axes of a pentagonal bipyramid. The axial positions are defined as 1(+X), 3(+Y), 5(+Z), 7(-Y), 9(-X), and 12(-Z); the Y and Z axis pairs align along the vertices of an approximately planar pentagon, and the x-axis pair takes up an axial position perpendicular to the Y/Z plane [65]. Figure 4 demonstrates the EF hand calcium binding loop (functional loop) and the amino acids involved in the coordination of the calcium ion.

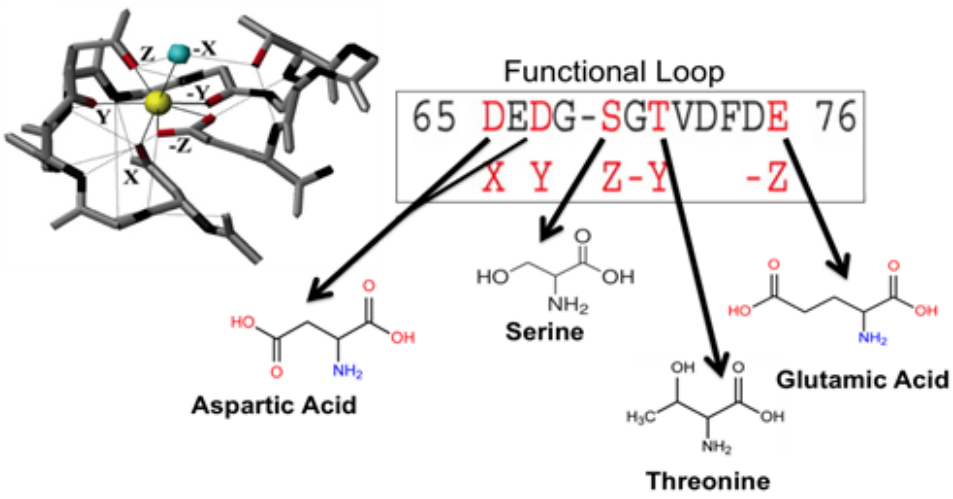

Figure 4. A representation of Ca^{2+} ion coordination in a functional calcium binding EF hand loop. The amino acids used to coordinated calcium within the EF loop are highlighted in red with their structures shown [32,65].

Based on the canonical definition of the EF hand loop, aspartic acid is the preferred chelating residues at positions 1, 3, 5 and 9 while the carbonyl group of threonine and glutamic acid are shown to coordinate Ca^{2+}at position 7 and 12 respectively. These amino acids strategically arrange to coordinate calcium in a pentagonal bipyramidal geometry, most commonly known as the canonical geometry for EF hand sites [32]. This geometric structure is further supported through a network of hydrogen bonds established through the ligands, both between and around the EF hand calcium binding loop. These additional interactions help stabilize the unfavorable close proximity of the negatively charged oxygen atoms in the coordination sphere of the bound Ca^{2+} [65].

Although studies have demonstrated that the coordinating ligands in the EF hand loop can vary between species, these sites are shown to continue to bind calcium in a pentagonal bipyramidal geometry. This is most likely due to the additional stability achieved in the protein structure when the ligands orient on the appropriate axis to coordinate the incoming Ca^{2+} [32,33,48].

EF hand proteins that coordinate calcium in geometric arrangements that differ from the canonical standards are referred to as non-canonical EF hand loops, and are considered to coordinate calcium with a non-canonical geometry. These EF hand proteins have been shown to coordinate calcium in a pentagonal bipyramidal fashion through amino acids that differ from those of the canonical loop. In most cases this is a due to an amino acid insertion in the EF hand loop, or because the EF loop is shorter than the canonical sequence [65].

In addition, some EF hands have shown to coordinate Ca^{2+} with an octahedral geometry, although Ca^{2+} is rarely found to exist in this coordination arrangement in EF hand sites. The octahedral geometry is commonly preferred in EF hand sites when binding magnesium ions [65].

This is most likely due to magnesium ion's smaller ionic radii, which prevents direct coordination of the 12th amino acid in the EF hand loop. When aspartic acid is found at this position, a water molecule is normally present to bridge and strengthen the interaction between the metal ion and coordinating ligand; as a result an octahedral geometry is achieved [65].

The geometric coordination arrangement achieved by the EF hand loop depends on the canonical amino acids that chelate Ca^{2+} directly. These residues play a huge role in stabilizing and facilitating the folding of the protein structure and are often conserved between species. For example, aspartic acid is one of the most highly conserved amino acids of the EF hand loop due to its versatile role: it provides both the structural and conformational arrangements of the protein needed to interact with calcium ions. Aspartic acid residues most commonly serve as coordinating ligands for Ca^{2+} due to the preference of the EF hand loop for carboxylate ligands with a less bulky side chain [75].

When comparing the amino acid sequences of various EF hand loops from a range of species, the aspartic acid at position 1, 3 and 9 remains consistently conserved. At the first coordination site (+X position of the pentagonal bipyramidal geometry), the aspartic acid provides the precise stereochemical arrangement needed for the protein to properly coordinate a Ca^{2+} ion in the EF hand loop. This arrangement positions the carboxylate oxygen atoms of the resides so they are available to interact with various other amino acids within the same loop [65] As a result, this creates an extensive hydrogen bonding network within the loop which further stabilized the protein structure as it transitions to a calcium bound state [65]. The precise steric dimensions of this side chain are pivotal for coordinating calcium in the EF hand loop, as previous studies have shown that if an amino acid residue other than aspartic acid present at position 1 in the EF hand loop will not bind calcium [32].

The overall effects induced on the protein through the different interactions occurring between the aspartic acid and the other residues at each position in the loop is due to the position of aspartic acid in the loop. Utilizing aspartic acid at these positions provides the most suitable environment for the loop to coordinate calcium, and as a result, optimizes the overall function of the EF hand [75].

Another commonly conserved location for Aspartic acid in the EF hand loop is at positions 3 (-Y) and 9 (-X). At position 3 the aspartic acid residue interacts with calcium through the carboxyl group in the C –terminal and on the R group of the amino acid. This allows the aspartic acid residue to fluctuate between a mono-dentate and bidentate ligand to calcium, which provides flexibility to the loop and creates a more versatile role in coordinating metal ions.

Additionally, Aspartic acid is found 23% of the time at position 9 (-X) in EF hand proteins. At this position Ca^{2+} is either chelated directly, or indirectly through a bridged water molecule, to the aspartic acid residue. This residue is shorter than glutamic acid, which is also found to exist in this position of the EF loop in some species. In order to accommodate the smaller side chain of aspartic acid, a water molecule is incorporated into the coordination sphere to help bridge the interaction between the loop and the calcium ion. The specific nature of residue 9 seems to be one of the major factors that control the rate of Ca^{2+} binding and release, and thus also affinity of the EF hands [64,65].

Aspartic Acid is also found at position 12 of the loop, but is not preferred at this site. Instead glutamate is more commonly found at this position due its larger coordinating group size. The small size of the aspartic acid residue creates a large gap between the coordinating atoms of the ligands and the metal ion. A water molecule is inserted to bridge this interaction but as a result, the affinity and ion selectivity for calcium in the EF hand loop site is significantly

decreased [65]. To avoid these effects on the protein, glutamate is most often used as the cleating residue at position 12. Glutamate's larger size allows the coordination atoms come into close proximity of the metal ion so that the amino acid can serve as a bidentate side chain ligand in the (-Z) plane of the pentagonal bipyramidal geometry of the calcium bound EF hand. As a result, a stronger and more stable interaction is achieved in the EF hand loop.

Threonine is an additional canonical amino acid, most commonly found at the 7^{th} position in the EF loop. This amino acid provides the (-Y) part of the coordination geometry where the backbone carbonyl is used in chelating Ca^{2+}. It was found through NMR studies utilizing paramagnetic lanthanide derivatives revealed that the 7^{th} position in the EF2 loop of CaM had a tendency to gain an extra water molecule as a ligand; this coincided with a decreased contribution from the main-chain carbonyl group [76]. Ultimately, this ligand exchange results in two water molecules in the coordination sphere, which increases the flexibility of the loop [76].

The non-chelating amino acids of the EF loop also play a pivotal role in maintaining the structural integrity of the EF hand domain. The positions in the loop that do not provide direct chelating residues, but are crucial for proper protein folding and arrangement, include positions 6 and 8. Glycine is highly conserved in EF hands at position 6 of loop, primarily due to its small size which facilitates the unusual main chain conformation (φ and ψ angles of 60° and 120° respectively). Upon binding calcium to the EF loop, the presence of glycine enables the 90° turn which allows the remaining calcium ligands to coordinate. Additionally, glycine, as seen in triplet in the N -terminal EF hand loop of sTnC, is more disordered and thus more stable in terms of conformational entropic free energy than EF loop II [77,78].

Ordering EF loop I gives it a 10 fold lower affinity for calcium when compared to EF loop II [79].

The hydrophobic residue at position 8 [80] is also a highly conserved non-calcium chelating amino acid. Its role in the EF hand loop is to participate in the formation of short antiparallel β-sheets with the corresponding paired loop's eighth position. This interaction is known as the β-scaffold and will be discussed further in the subsequent section.

1.5.3 EF Hand Pairs and β-Scaffold

EF hands are normally found to in pairs; they are joined through hydrogen bonding interactions that occur between the backbones of the EF hand loops (Figure 5). These interactions form local anti-parallel β-sheets, termed the EFβ-scaffold, and are known to serve two purposes: stabilize the two EF-hands and govern the Ca^{2+} induced conformational change of the protein (Figure 5). Residues in the –Y position, and the hydrophobic amino acid (Ile, Val, or Leu) adjacent to the residue in the –Y position, are known to be involved in the hydrogen bond network between the main chain NH and CO groups. This interaction forms the basis of the β-sheet. In the Ca^{2+} bound form, stability of the EF hand pair is achieved through the hydrophobic interactions occurring between the non-polar amino acids of the alpha helices adjoining the calcium binding loop.

Multiple EF hand pairs are found in various calcium binding proteins. The EF hand pairs in these proteins tend to form globular domains [66]. These globular domains can either act independently from one another, as in the case of CaM and TnC, or they can be well packed, resulting in a single oval shape and act as a cooperative unit as seen in the structure of recoverin [81-83].

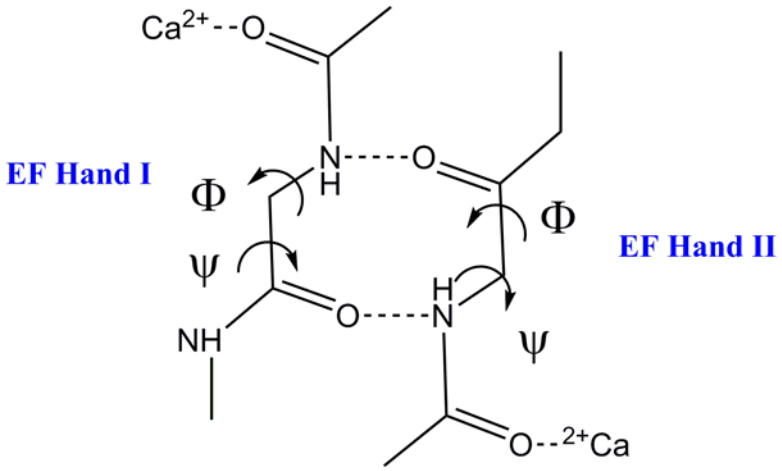

Figure 5. A representation of the molecular interactions occurring between two EF hand mates. The hydrogen bond network shown constitutes the β-scaffold between the two calcium binding loops. *Figure adapted from reference* [84].

1.5.4 The Mechanism of Ca^{2+} Binding

A two-step model, termed the EF-hand β-scaffold (EFBS) model, describes the Ca^{2+} binding mechanism [84]. According to this model, Ca^{2+} first binds to the N-terminus of the loop. This ion is held in position because of the structural rigidity of the β-sheet, achieved as a result of the relocation of the alpha helices that make up the EF hand motif. This conformational change causes the EF helices to form an area of positively charged amino acids, which then polarizes the bond network (EF-β scaffold) and facilitates the interaction of the EF-hand mates. As a result, stabilization is achieved in the structure of the EF hand pair.

In the second step, Ca^{2+} binding to the EF hand loop induces a helical transition between the backbone phi and psi angles of the amino acids that make up the EFβ-scaffold. This further causes a rotation between the C-terminus of the Ca^{2+} binding loop and F helix that differs by

approximately 2Å [83]. As a result of this shift, the bidentate Glu at position 12 of the loop, is close enough to interact with the calcium ion through electrostatic interactions. This further re-positions the oxygen atom located in the equatorial plane of the Ca^{2+} ligand complex, and allows the calcium ions to coordinate in the loop with the canonical pentagonal bipyramidal geometry.

The EFBS model describes how the EFβ-scaffold allows two Ca^{2+} ions to bind to the two EF hand domains with positive cooperatively. This is observed in the C-domain of various EF hand proteins [66]. When calcium binds to EF hand loops of the C-domain in skeletal TnC, the loop closes around the calcium ion as the inter-helical angles of the E and F helices decrease from 135° in the apo form to 90° in the Ca^{2+} bound form. The E and F helices shift from an antiparallel orientation to perpendicular relative to one another. The movement of one EF-hand is "felt" through the network of hydrogen bonds by its EF-hand mate. As a result the second loop opens which facilitates a calcium ion to bind to that EF hand site.

This structural transition is highly important for EF hand proteins to carry out their appropriate function. This is apparent in troponin C, a muscle regulatory protein that relies on this coordinating movement to successfully interact with target proteins in order to maintain and control muscle movement [78].

1.6 Troponin C

Troponin C is a member of the superfamily of EF hand calcium binding proteins [62] and participates as the regulatory subunit in a heterotrimeric troponin complex to facilitate muscle contraction and relaxation in both skeletal and cardiac muscle. The binding of Ca^{2+} to TnC initiates a cascade of conformational changes through the component proteins of the thin filament, leading to the formation of cross bridges (CBs) between actin and myosin and the

generation of force by the myocyte. Therefore, the functional properties of TnC, including its ability to be activated by Ca^{2+}, have significant regulatory influence on the contractile reaction of the myocyte.

TnC has two EF hand pairs, one at the C domain and one at the N domain as demonstrated in Figure 6. The EF hand loops that compose both domains are referred to as EF I (Site I) through EF IV (Site IV) where EF I and II (Site II) are located in the N domain and EF III (Site III) and EF IV are found in the C domain of TnC. The EF hand loops and their corresponding amphipathic helices referred to as helices A and B, C and D, E and F and G and H respectively [66], form a four helix bundle with their helices packed together to make a hydrophobic core [65]. This hydrophobic region is exposed upon calcium binding to the EF hand sites and serves as subsequent binding sites for target proteins. The EF hand sites and corresponding helices are shown in Figure 6.

Connecting both globular domains of TnC is an alpha helical linker region [65]. As demonstrated in skeletal and cardiac muscle cells, the helix-loop-helix motif of the EF hands allow TnC to act as a Ca^{2+} sensor whereas the linker region provides a way to relay the calcium signal throughout the thin filament [65]. The C and N terminal domains bind calcium with different affinities affecting the overall conformational movement between each region of the protein. The C-terminal EF loops bind calcium with a high affinity for structural purposes, whereas the N-terminal has a lower affinity for calcium as a mechanism of protein regulation [52,65]. It is the binding of Ca^{2+} to the regulatory domain EF sites that induces a change in HcTnC conformation that modifies subsequent protein-protein interactions in order to activate muscle function.

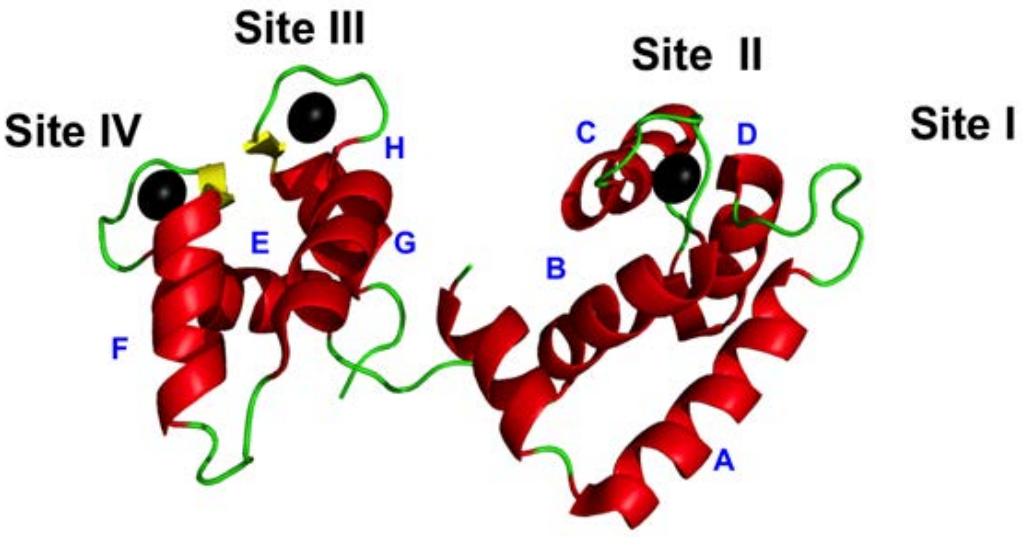

Figure 6. Structure of full length cardiac TnC showing the C (Left) and N (Right) domains of the protein. Each EF hand is labeled as sites I through IV. Both regions are separated by a linker regions highlighted in green. The helices corresponding to each EF hand are labeled in blue. PDB 1AJ4 [85].

Within a myocyte or muscle cell, TnC is present in complex with Troponin I (TnI) and Troponin T (TnT). The troponin complex is bound to tropomyosin, which is bound to both sides of actin along the helical groove. The orientation of tropomyosin on actin is controlled by calcium as it alters the interactions within the troponin complex and among actin and tropomyosin Increased intracellular calcium concentration from approximately 100 nm triggers the low affinity sites in the N -terminal domain of TnC to bind calcium [54]. This induces a conformational change in the N domain of cTnC that partially 'opens up' and exposes the central hydrophobic cavity of the EF hand pair. This exposed region is thought to strengthen the interaction between TnC and the "switch" region of TnI (residues 147–163) [54]. Consequently, the interaction between actin and the inhibitory region of the TnI (residues 128–146) decreases

[86]. As a result, the inhibitory region of TnI detaches from actin. This change produces structural changes in actin [87] that are thought to be important in the regulation of ATPase activity.

In addition, calcium binding to TnC facilitates tropomyosin to move from the inhibitory position to the active position on actin. This results in an increased affinity of rigor myosin and myosin-ADP binding to actin. Myosin, a hexamer protein composed of 2 heavy chains and 4 light chains, contains two globular head regions that contain both ATPase activity and actin-binding activity. The energy released from hydrolysis provides the power needed to facilitate muscle contractions. Although the movement of tropomyosin does not have a large effect of myosin S1 binding during steady state ATP hydrolysis [88], there is an increase in the k_{cat} for actin activated ATPase activity of about 25-fold [89]. Therefore, the strength of these interactions between actin and myosin at the actin-binding sites, as well as the rate of CB cycling, and the rate of ATP hydrolysis by myosin ATPase [90], together, influence Muscle contractility.

Muscle contraction is an ATP hydrolysis driven, cyclic interaction, of myosin and actin [91]. ATP hydrolysis occurs yielding an ADP and P_i molecule when ATP binds close to the myosin head projections [91]. Myosin then binds to actin which initiates hydrolysis of ATP, thereby releasing a P_i molecule into the cytosol of the cell [91]. The energy released as a result of ATP hydrolysis causes the myosin heads to propel the actin back toward the tail of the myosin, allowing actin and myosin to slide along each other [91]. Once this process is complete, ADP is released from myosin and the head discharges from actin [91]. As long as calcium is present, ATP binds once again to the Myosin domain and the process continues. Figure 7 provides a

representation of the proteins units involved in muscle contraction and their relative positions to one another under non-calcium conditions.

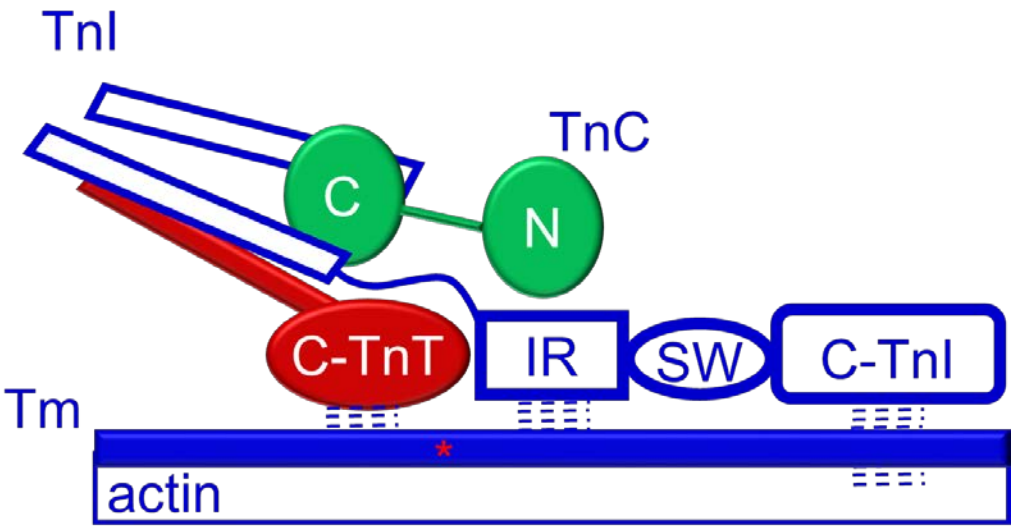

Figure 7. Representation of the interactions between the regulatory proteins involved in cardiac muscle function, under non-calcium conditions. (Filled dumbbell) TnC. (Bold Lines) Two TnI helices and the inhibitory region (IR), the switch region (SW), and the C-terminal region between residues 164 and 210 (C-TnI). (Black) TnT helix and the C-terminal region encompassing residues 271–288 (C-TnT). (Parallel dotted lines) Possible interactions occurring with actin and tropomyosin (Tm) when Ca^{2+} is not bound to TnC, actin is known to be associated with the inhibitory, and C-terminal region of TnI, which inhibits specific binding sites on actin for myosin. *Figure adapted from reference* [92].

1.5.1 Skeletal versus Cardiac TnC

Troponin C serves as an important protein for the regulation of muscle contraction and can be found in both skeletal and cardiac muscle. There are distinct differences between sTnC and cTnC which make them specific for the tissues in which they reside. CTnC and sTnC are both small (161 and 162 amino acids, respectively) dumbbell-shaped proteins composed of two Ca^{2+} binding EF hand domains separated by an alpha-helical linker [93], both containing the same number of EF hand sites [94].

The low-affinity NH_2-terminal domain contains Ca^{2+} binding sites I and II, and the high-affinity COOH- terminal domain contains Ca^{2+} binding sites III and IV [93]. All of these EF hand sites in sTnC bind calcium. However, in cTnC, the first EF hand (loop I) is considered nonfunctional; it will not bind calcium due to amino acid sequence substitutions that have occurred within the metal binding loop [93]. Comparing the EF I loop sequence with canonical EF-hand loop sequences, substitutions of the residues at positions 1 and 3 are replaced by two nonpolar residues (Valine and Leucine) that are unable to coordinate Ca^{2+} ions [95,96].

EF hand II, also known as the functional binding site, mimics the loops of the C-domain in amino acid sequence and structure of both isoforms allowing Ca^{2+} to bind. EF II then serves as the sole Ca^{2+}-binding site in N-cTnC at physiological Ca^{2+} concentrations and acts as the lone Ca^{2+} sensor in the troponin complex for cardiac muscle function [97]. This differs from sTnC which utilizes calcium binding in both EF hand sites. Cardiac TnC proteins isolated from other mammalian species have also been shown to contain a nonfunctioning (non-calcium binding) loop I, which makes this a unique variation for cTnC [93]. The EF hand II of TnC consists of a 12-residue loop region [98] which forms a pentagonal bipyramidal arrangement around the Ca^{2+} ion and are at positions X, Y, Z, -Y, -X, -Z [98]. When comparing the functional calcium binding

sites in sTnC and cTnC, the metal binding arrangement remains consistent, thereby suggesting that this arrangement is native to EF hands and TnC.

Even though the tertiary structure of the regulatory region of sTnC and cTnC has been relatively retained [99] the functional properties of the Ca^{2+} binding sites of these different proteins have been altered through sequence manipulation. In addition to the nonfunctional loop in cTnC, the amino acids of the functional loops vary between isoforms. As a result, the two TnC analogs have different affinity for Ca^{2+} ion and are activated by the metal ion differently. For example, previous studies involving one-dimensional ^{1}H and two-dimensional $\{^{1}H,^{15}N\}$-HSQC NMR spectroscopy have demonstrated that the Ca^{2+} affinity of chicken skeletal NTnC loop II is approximately 2 fold the affinity of cTnC human site II [97]. Also, the hydrophobic patch exposed following Ca^{2+} activation with sTnC is 500 Å in area on the surface of the NH_2 terminus [79].

In contrast, the hydrophobic patch exposed upon the Ca^{2+} activation of cTnC is 18 Å [79]. This hydrophobic patch does not open to a comparable degree until cTnC interacts with the switch region (residues 147–163) of TnI peptide which causes an increase in the opening to 162 Å [79,86,100]. These results can be attributed to cTnC having only one functional Ca^{2+} binding site (loop II). This causes sTnC and cTnC to demonstrate distinct responses to Ca^{2+} binding to the N-domain. The binding of Ca^{2+} to loop I in sTnC causes a rearrangement of residue side chains that contributes to the enthalpy required to overcome the energy barrier of exposing the hydrophobic core [100]. Since this site does not bind calcium in cTnC, comparatively, the hydrophobic patch is not as exposed. As a result, cTnC is dependent on the interaction with cTnI to facilitate the hydrophobic core to open.

In addition to the differences stated above, cTnI also contains a 32 amino acid (31 in human) N' extension that is absent in the slow skeletal TnI isoform [101]. This extension consists of three regions; an acidic N' region containing a single turn helix, an extended proline helix, and a C' helix containing a bisphosphorylation motif (Ser23/24) [102][103]. Phosphorylation of these two serine residues by cAMP-dependent protein kinases occurs in response to β-adrenergic stimulation of the heart and provides a mechanism to fine tune contractile function [104-108]. Effects of bisphosphorylation include a reduced affinity of Ca^{2+} for cTnC [109,110], a reduction of myofilament Ca^{2+} sensitivity [111], as well as an acceleration in cross-bridge cycling [112].

Studies probing the interaction between cTnI and cTnC have demonstrated that the N'-extension interacts weakly with the regulatory domain of cTnC, presumably stabilizing more open and hence active conformations [113-116]. The proposed binding region of the N' extension occurs between residues 22 to 34 [117,118] while the putative binding site in the N lobe of cTnC is localized on the β-sheet bridging Ca^{2+} binding loops I and II [115,116]. Phosphorylation at serine residues 23 and 24 appears to abolish binding to N-cTnI [113,115-117].

1.6.2 Cadmium Binding to Cardiac TnC

The metal binding sites in EF hand proteins are normally rich in hard base atoms, such as oxygen, to provide an environment chemically compatible to coordinate a Ca^{2+} ion. However, it has been noted that these oxygen ligands can be mutated or replaced by residues that contain soft base ions such as sulfur [26,56,119]. These variations can effectively decrease the affinity or inhibit these sites from coordinating calcium, an example being the previously discussed EF I

metal binding site in the N-domain of cardiac TnC. This site is considered nonfunctional, or non-calcium binding, due to the presence of a cysteine residue located at position 7 of the loop [32]. The presence of this cysteine residue makes this site suitable for interactions with soft acid ions such as toxic metal, Cd^{2+}.

The structure of the human N-cTnC domain has been studied extensively by NMR [85,86,120,121] but few crystal structures of N-cTnC are available owing to difficulty in forming ordered crystals. Cd^{2+} has been used in these structures provide N-cTnC crystals that diffract to high resolution [33]. Through using Cd^{2+} for crystallization, it has been found that Cd^{2+} can coordinate with Ca-binding proteins, as demonstrated by a recent study that found Cd^{2+} bound to both the regulatory loop, EF II, and vestigial site, EF I, of WT human N-cTnC [52].

The Zhang lab demonstrated that the EF hand loops, I and II, of the N-terminal in cTnC were shown to bind Cd^{2+}. The EF II loop, or functional Ca^{2+} binding site, is shown to bind Cd^{2+} in a canonical pentagonal bipyramidal geometry with a partially disordered binding loop. This distorted geometry is a result of water molecules replacing the coordinating residues Asp67 (Y) and Ser69 (Z). The non-metal binding EF -I loop, or the 'defunct loop' also binds the Cd^{2+} ion, but does so in a 'distorted' octahedral geometry. There is evidence of EF hands having the ability to bind calcium in an octahedral geometry, but this is a non-canonical arrangement. However, it is usually observed that Cd^{2+} is bound to non-EF hands with octahedral geometries [33].

The EF II site in cTnC coordinates Cd^{2+} in a canonical but distorted pentagonal bipyramidal geometry, with four of the ligands coming from Asp65 O(X), Thr71 O (-Y) and Glu76 O/O(-Z) and three others from water molecules (-X, Y and Z) (Figure 8). Since two of the conserved residues, Asp67 (Y) and Ser69 (Z), are not observed in the electron density (they are presumably in a dynamic state), water molecules substitute for the disordered ligands. To our

knowledge, this is the first time such an ion coordination has been observed in the N domain of cTnC or any other EF-hand protein. This reveals tremendous flexibility in the ion-coordination repertoire of this protein. Although NMR data and previous crystal structures have demonstrated Cd^{2+} coordinating in the canonical pentagonal bipyramidal geometry in the EF hand sites of Parvalbumin, the C domain sites of sTnC. Figure 2 compares the structures of these proteins, as well as the N-Terminal domain of cTnC with Cd^{2+} bound to the Ca^{2+} binding sites of the protein.

The Cd^{2+} ion located in EF-hand I of cardiac TnC was shown to coordinate with six ligands thus leading to a non-canonical, 'distorted,' octahedral geometry. Cd^{2+} is coordinated in this manner by binding to the: main-chain carbonyl oxygen of Cys35 (X), oxygen from a water (–X), main chain carbonyl oxygen of Asp33 (Y), amino acid residue oxygen Asp33 (Z), sulfur at Cys35 (-Y) and acetate (OXT) at the -Z position. The covalent bond formed between Cd^{2+} and the S atom of cysteine is thought to inhibit Cd^{2+} from dissociating from EF I once it is coordinated, thereby indicating a possible irreversible toxic effects of cadmium [32].

It has been established that five EF-loop residues at positions 1, 3, 5, 7 and 12 contribute coordinating ligands to the calcium ion. However, In EF I of the structure presented here in Figure 8, only two residues, Asp33 and Cys35 (positions 5 and 7), contribute to Cd^{2+} coordination. As mentioned, the EF I loop in cTnC does not normally bind ions (vestigial site); however, the structure in Figure 8 shows that EF I manages to coordinate Cd^{2+} by changing the loop conformation. This also causes the side chain of the glutamate residue at position 12 to change its spatial arrangement. The Glu12 side chain is shown to point away from the coordination site and is therefore not available for coordinating Cd^{2+} in the canonical fashion. This feature can be observed by comparing the EF I coordination (listed in Table 3) between the N terminal of cTnC with and without bound deoxycholate (DXC).

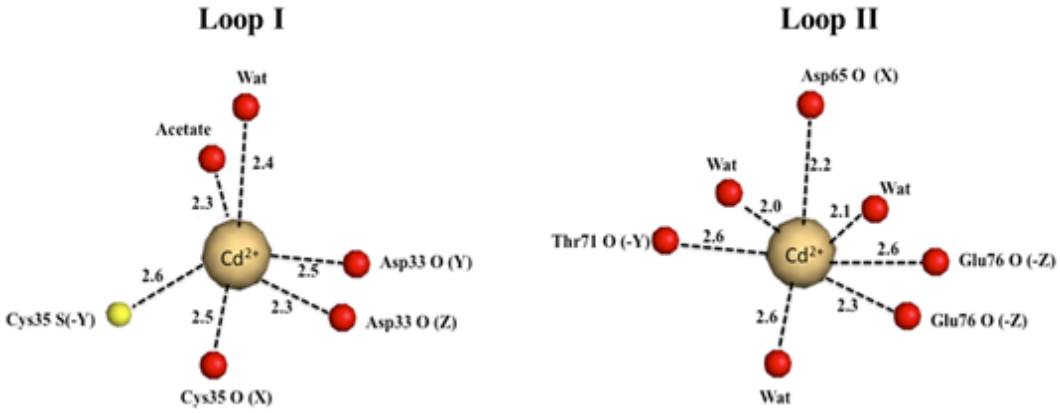

Figure 8. Cadmium coordination in the N terminal EF hand sites of cTnC. Cd^{2+} coordinates in the EF I hand loop in a non-canonical, 'distorted,' octahedral geometry through interactions with residues Cys35 (X, -Y), Asp33 (Y), and Asp33 (Z) of the loop as well a water molecule (–X), and a main chain acetate (OXT) (-Z) ion. EF II in cTnC coordinates Cd^{2+} in a canonical but distorted pentagonal bipyramidal geometry. Coordination at this site is achieved with four of the ligands coming from Asp65 O(X), Thr71 O (-Y) and Glu76 O/O(-Z) and three others from water molecules (-X, Y and Z). *Figure adapted from references* [32,33].

Other data have verified that EF II in in the N domain of cTnC–DXC and EF II in the N-cTnC structure presented here both coordinate Cd^{2+} in the canonical fashion [33]. The two EF loops in skeletal troponin C also coordinate Cd^{2+} canonically [57] leading to the conclusion that Cd^{2+} ions are able to substitute for Ca^{2+} ions in EF hands in a canonical fashion. Indeed, functional data show that Cd^{2+} can activate skeletal troponin C (in which EF I is functional) by substituting for Ca^{2+} [85,94].

By comparing the EFI loop sequences of parvalbumin, calpain, sTnC, cTnC, it can be seen that cardiac troponin C is the only one with cysteine as a coordination residue; bear in mind

that the cysteine is coordinating a Cd^{2+} ion in a vestigial ion-binding site, so its significance is not clear in a physiological sense. To our knowledge, there is no other example of an EF hand protein in which cysteine serves as an ion-coordinating ligand. Interestingly, the NMR structural data for cardiac TnC with Cd^{2+} bound has a similar overall conformation to that observed when Ca^{2+} bound NMR structures [85].

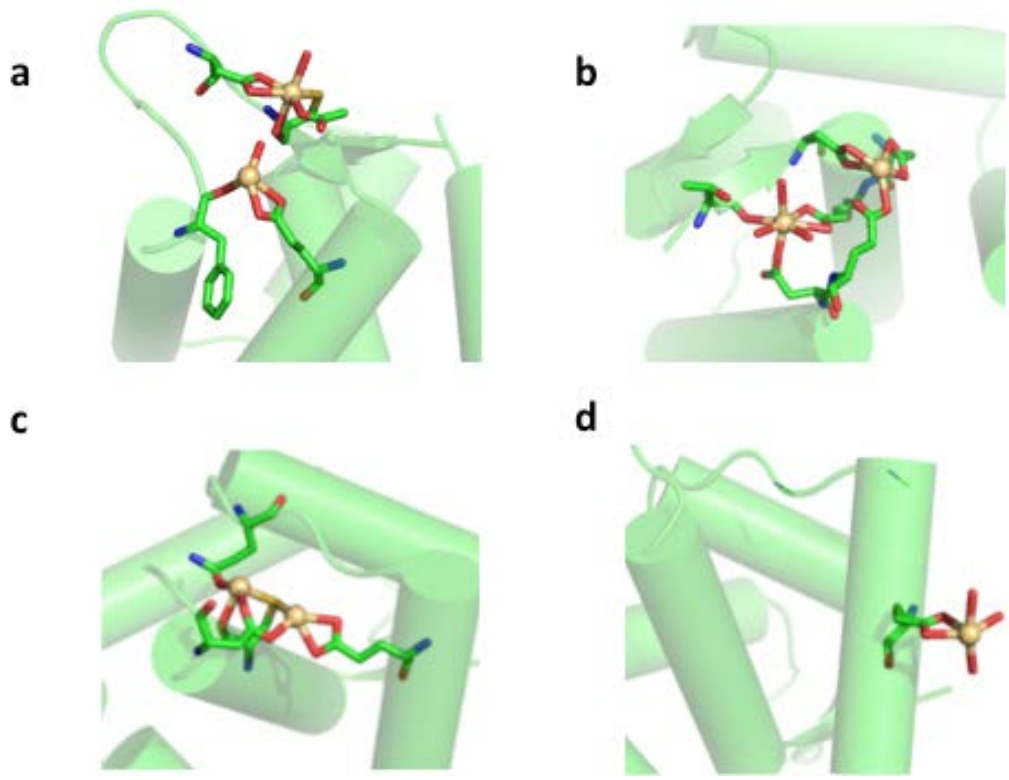

Figure 9. Crystal structure of HcTnC1-89 highlighting various Cd^{2+} coordination sites (PDB ID 3SD6). (a) Cd^{2+} ions bound to loop I. Top Cd^{2+} ion coordinated to Cys35 (S and amide O), Asp33 (O δ1 and δ2), 1 Wat, and Acetate. Bottom Cd^{2+} ion coordinated to Glu40 (O ε1 and ε2), Phe27 (amide O), and 1 Wat. (b) Cd^{2+} ions bound to loop II. Left Cd^{2+} coordinated to Glu76 (O ε1 and ε2), Thr71 (O), Asp65 (O δ2) and 3 Wat. Right Cd^{2+} coordinated to Asp73 (O δ1 and δ2) Asp75 (O δ1 and δ2), and Glu66 (O ε2). (c) Binuclear Cd^{2+} center bridged by Cys84 (S). Left Cd^{2+} bound to Asp87 (O δ1) and Gln50 (O ε1). Right Cd^{2+} bound to Asp87 (O δ2) and Glu56 (O ε1 and ε2). (d) Cd^{2+} coordinated to Glu59 (O ε1 and ε2) and 3 Wat.

Due to its filled d^{10} orbital shell, and empty f^{14} orbital, cadmium can easily donate or accept electrons from other atoms thereby creating a variety of interactions with surrounding molecules. As a result, cadmium can take on a number of different coordination geometries in a

variety of metal binding sites, even if those sites are designed to coordinate metal in a specific manner.

Examination of non-EF-hand proteins in complex with Cd^{2+} reveals that Cd^{2+} is most often coordinated in either tetrahedral or trigonal bipyramidal geometries, with histidine and cysteine residues most frequently involved in coordination. It has been reported that Cd^{2+} was also involved in an octahedral geometry using histidine residues as coordinating ligands [122]. Other geometries, such as trigonal bipyramidal, have also been observed with Cd^{2+} coordinating through interactions with two cysteine residues, one histidine residue, and two water molecules [14,49-51,123,124]. The ionic radius of Cd^{2+} is similar to that of Ca^{2+}; this similarity in size and charge make the two ions competitors for the same protein ion-binding sites [125,126].

Finally, Cd^{2+} appears to be more flexible in its coordination number and geometry than Ca^{2+}, thus allowing cadmium to accommodate protein conformations in calcium binding sites or in sites in which metal binding does not occur. These interactions may impose a threat to the function of the protein which in turn could have detrimental effects on the organ system and overall health of those organisms with elevated Cd^{2+} concentrations.

1.6 Project Goals

Although government regulation has helped control the amount of cadmium emitted into the environment and mobilized into food sources, the metal is persistent in the environment due to its continued use in manufacturing and its emission due to the petroleum and mining industries. Therefore, cadmium toxicity is still a major concern especially for those working in or near these industries and smokers. While mechanisms of cadmium toxicity are not known exactly, it is known that Cd^{2+} ion can effectively bind to and displace metal ions from a wide

variety of proteins including thiol containing and calcium binding proteins as previously discussed.

As mentioned above, recent crystal structures of Cd^{2+} bound to the regulatory domain of HcTnC ($HcTnC_{1-89}$) in the free and DXC bound states reveal interesting Cd^{2+} structures, two of which are bound to both Ca^{2+} binding loops. The most interesting aspect of these was the fact that Cd^{2+} was present in EF hand I loop, a region that does not bind Ca^{2+}. In light of the potential interactions that take place between the regulatory domain and other members of the troponin complex such as cTnI, the presence of cadmium at this site may disrupt these interactions.

It is therefore the goal of this research project to study the interaction between HcTnC and Cd^{2+} carefully by using isothermal titration calorimetry (ITC). We used ITC to determine the thermodynamics (G, H, and S) of Cd^{2+} binding to both full length HcTnC and the regulatory domain, $HcTnC_{1-89}$. The data were compared to Ca^{2+} titrations under identical conditions. Further displacement titrations were performed whereby one metal was titrated into protein containing the other and vice versa. Data obtained indicated stoichiometry, and allowed for the elucidation of putative cadmium binding sites.

Chapter 2: Experimental Methods

2.1 Isothermal Titration Calorimetry

Isothermal titration calorimetry (ITC) is a useful technique used to determine the binding affinity and thermodynamic parameters of a reaction between two or more molecular species. It does so by measuring the amount of heat generated or absorbed from each binding event occurring between molecules in a given solution. The data obtained from this method is typically fit using a mathematical model which further calculates the binding affinity between the two molecules, and the thermodynamic parameters stoichiometric ratio (n), binding constant (K), enthalpy (ΔH) Gibb's free energy (ΔG), and entropy (ΔS), of the reaction [127,128].

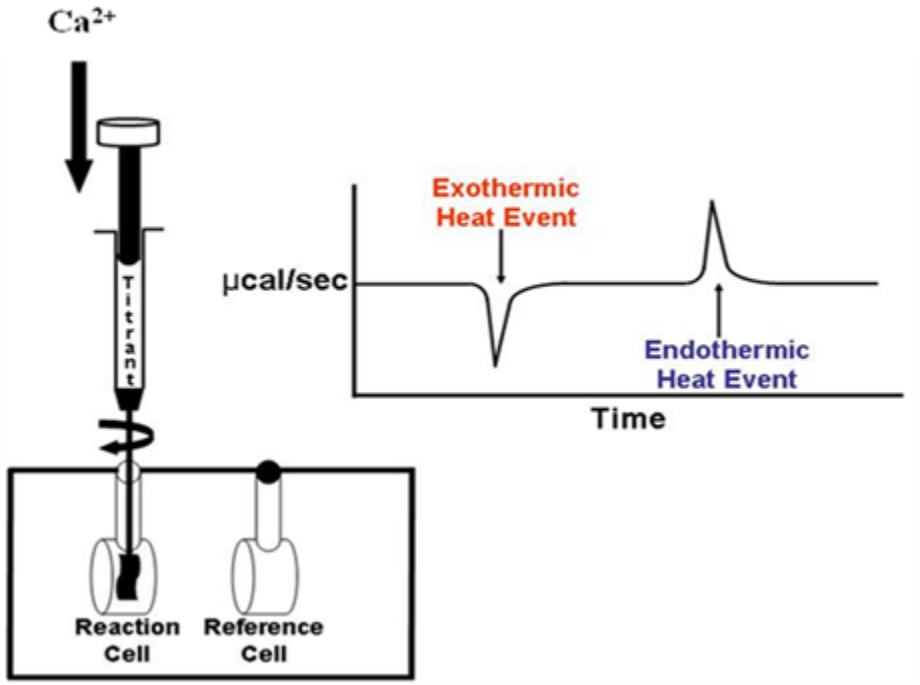

Figure 10. A diagram of a typical ITC experiment (Wilcox group, 2008).

2.2 ITC Instrumentation

ITC instruments are designed to efficiently measure the change in heat of a reaction, typically between a small ligands and a macromolecule, such as proteins. The data obtained using ITC is primarily achieved through the integrated design of the thermal core region of the instrument. Within this region there are two identical cells, known as the reference and reaction cell (Figure 10 & 11). These cells are composed of thermal conducting material protected by an adiabatic coating, known as the "jacket". This coating fills the internal space of the instrument and contains highly sensitive thermopile/thermocouple circuits which span throughout the entire region of the jacket. During a typical ITC experiment, the reaction cell, filled with a solution containing a specific protein or biomolecule, is titrated with precise aliquots of a known metal solution at specific time intervals throughout the reaction. The reference cell, usually filled with water or buffer solution, resides in close proximity to the reaction cell and is kept at a constant temperature throughout the duration of the experiment.

As titrant is added to the reaction cell, the two molecules begin to interact, and as a result, heat is either released into (exothermic) or absorbed (endothermic) from the surrounding solution. The highly sensitive thermoelectric device spanning the internal region of the calorimeter detects these thermal changes by measuring the difference between two separate temperature changes (ΔT_1 and ΔT_2) detected within the thermal region of the instrument. ΔT_1, is obtained by measuring the temperature difference between the reference cell and the jacket of the calorimeter, while ΔT_2 is calculated from the temperature difference detected between the reaction cell and reference cell [129,130]. The thermal region of the ITC instrument is shown in Figure 11 with the two differences in temperature denoted as ΔT_1 and ΔT_2, respectively.

During the course of a reaction ΔT_2 can fluctuate, since the amount of heat consumed/ produced from the reaction can change throughout the experiment. Therefore, in order to re-establish isothermal conditions, whereby the temperature difference between the two cells are held constant, the heat source controlling the reaction cell is adjusted accordingly using a cell feedback network (CFB) [130]. To elaborate, if a reaction cell produces heat (an exothermic reaction), the temperature of the system will increase. The calorimeter will sense this change and trigger a decrease in the power source. As a result, the temperature of instrument will decrease until isothermal conditions are re-established. The power required to maintain a constant ΔT_1 is integrated and divided by the total run time to obtain the function of the heat being observed [130]. These values are then plotted against time to produce the raw ITC data for a given experiment (Figure 12, top graph).

As the reaction takes place, the amount of heat absorbed or released from the reaction cell is measured and plotted on a graph. This energy change can differ with each binding event thereby producing a unique set of data points on the graph. For example, as demonstrated in Figure 12, a positive peak is observed in the raw data when heat is absorbed, which corresponds to an endothermic reaction occurring in the reaction cell. The energy lost during this reaction is compensated by an increase in power from the system, thereby resulting in positive peaks in the raw data. However, if heat is lost when the titrant is injected, a negative peak will result thereby corresponding to an exothermic heat event.

This quantity of heat absorbed or released during the mixing process is in direct proportion to the amount of binding. Therefore, as the protein reaches metal saturation, the heat signal diminishes until only heats of dilution are observed. The resulting isotherm is fitted using a binding model; from the fit, the thermodynamic parameters for the reaction can be obtained.

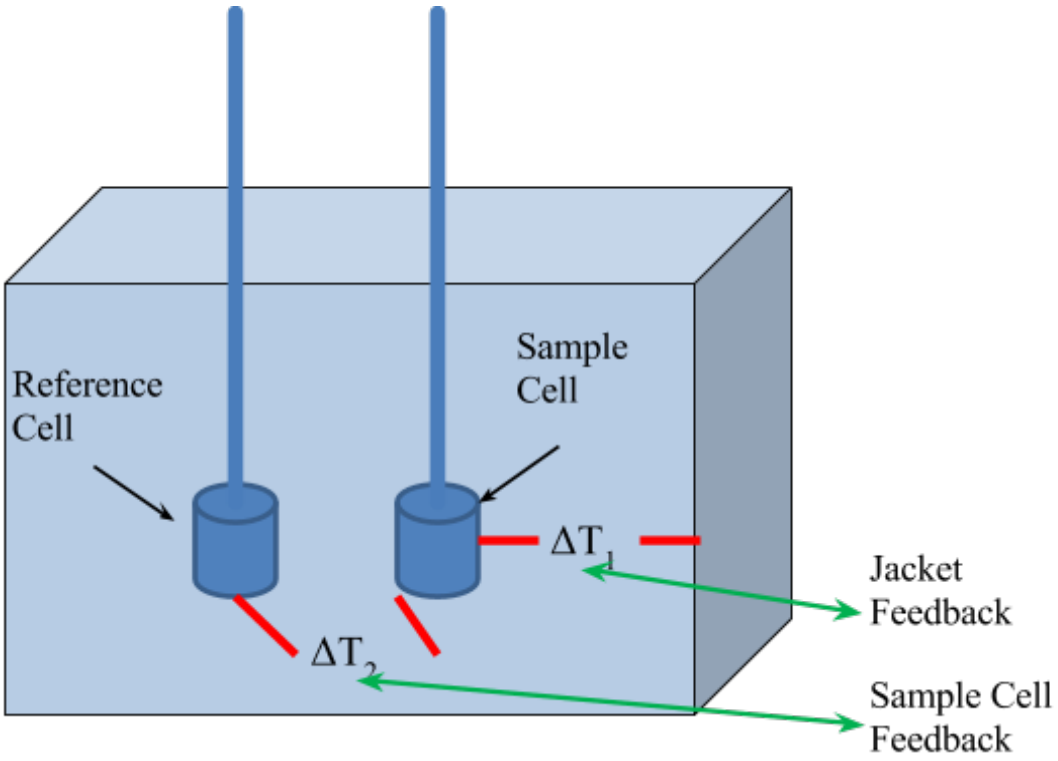

Figure 11. A schematic depicting both the reference and sample cell kept under isothermal conditions.

2.3 Thermodynamic Parameters

ITC is an effective tool used to determine the binding constants and thermodynamic parameters of interactions occurring in a solution. During a typical ITC experiment, a solution of small binding molecules is added to an analyte in small consistently portioned aliquots. The heat energy resulting after the solutions are mixed, is measured and reported as a peak on the raw data graph. These peaks represent a reaction that has gone to equilibrium since the peaks return to baseline after each injection. Integrating the peaks obtained from each injection (Figure 12, bottom

graph) provides a titration or binding curve of the reaction. Through further graphical manipulation the thermodynamic properties associated with the reaction can be extracted from the isotherm.

The binding affinity of metal to protein, along with the stoichiometry (n) and enthalpy (ΔH) of the reaction can be determined by applying a mathematical model to the binding curve from the titration.

From an ideal isotherm, the binding constant, or constants (K_B) of a reaction can be obtained from the slope of the fitted curve using equation 1. The parameters involved in this calculation include M, which denotes the concentration of the macromolecule, and X which represents the concentration of the ligand present in solution.

$$K_B = \frac{[MX]}{[M][X]} \qquad \text{Eq. 1}$$

The inflection point of the binding isotherm discloses the stoichiometry, n, of the binding of the titrant with the analyte while the difference in the heats associated with binding and the heat associated with the heat of dilution unveils the ΔH value of the binding.

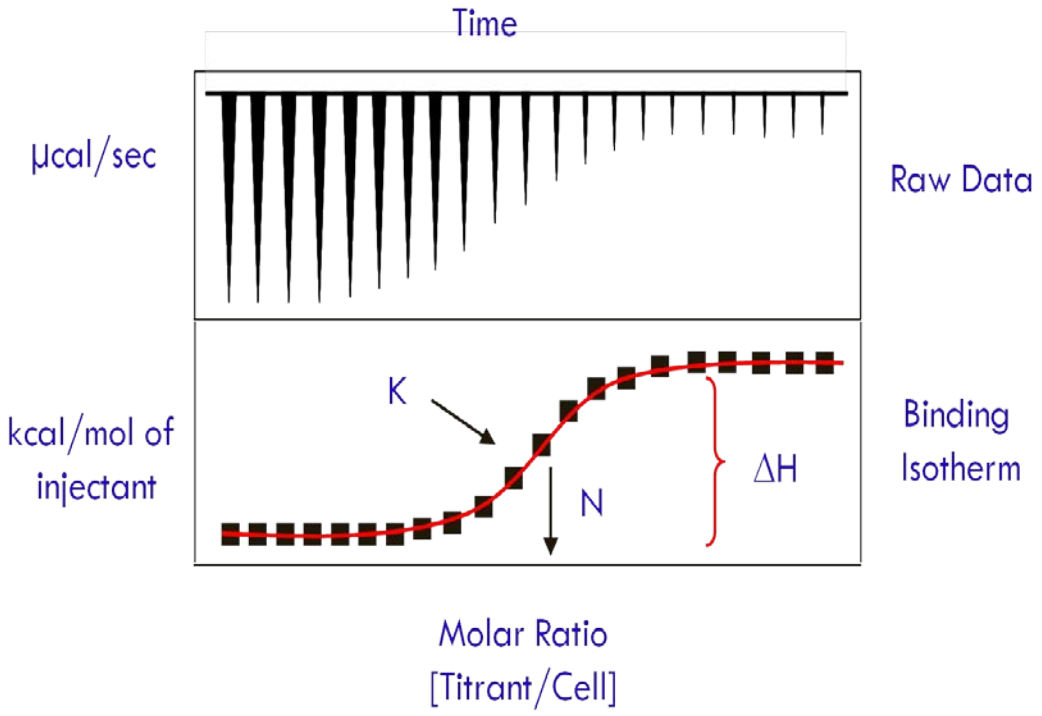

Figure 12. Representative data depicting an ideal exothermic thermogram. The raw data (top) and fitted binding isotherm (bottom) for a sample ITC experiment.

From K and Δ*H*, one can obtain a complete thermodynamic survey of the binding reaction by calculating the Gibbs free energy (Δ*G*), and entropy (Δ*S*) from the following equations:

$$\Delta G = -RT\ln(K) \qquad \text{Eq. 2}$$

$$\Delta G = \Delta H - T\Delta S \qquad \text{Eq. 3}$$

The variables include R, T and K which represent the ideal gas constant, temperature of the experiment and the binding constant obtained from the slope of the titration curve, respectively.

The change in Gibbs free energy (ΔG) represents the energy difference of a molecule in solution as it transitions from an initial to a final state, and is used to predict the direction and spontaneity of a reaction when conditions of a system are set at a constant temperature and pressure. A reaction with a negative ΔG is considered favorable/spontaneous and will occur without any additional input of energy. On the other hand, a reaction that yields a positive ΔG is deemed unfavorable/non-spontaneous and will not occur unless additional energy is added to the system. Reactions with a negative and positive ΔG are termed endergonic and exergonic respectively.

As demonstrated by the equation above, ΔG is dependent on the ΔH and Δ*S* of a reaction; these two thermodynamic parameters represent the forces driving a metal-protein complex formation [131,132]. Both ΔH and ΔS not only govern the overall ΔG value but provide a better understanding of the interactions occurring in a solution.

According to the second law of thermodynamics, energy is neither created nor destroyed. Therefore, during a reaction, the amount of energy available is proportioned throughout the solution until an equilibrium is established. The amount of energy transferred in a system through the formation and dissociation of bonds and intermolecular interactions is referred to as enthalpy. When bonds form, heat energy is released into the solvent, resulting in a negative ΔH value. The dissociation of bonds, however, require the consumption of heat, which results in a positive ΔH. The strength and amount of interactions can influence the enthalpy value while also providing insight into the interactions occurring in solution. For example, a reaction will favor a more negative ΔH if the bonds being formed are larger and stronger, than the amount of bonds dissociated in solution.

The entropy (ΔS) of a reaction is another important parameter to consider when calculating ΔG and when understanding the mechanism behind a particular binding event as it represents the dispersion of energy at a given temperature over microstates during a reaction. Processes that contribute to the entropy in a reaction include the hydrophobic effect, electrostatic charges, hydrogen bonds, conformational entropy, intermolecular vibrations and changes in equilibrium. Although, some of these processes are entropically driven processes, such as the hydrophobic effect, while the others, such as conformational entropy, are actual contributors to the total entropy. However, regardless the type of entropic process, they can all contribute to, or in some cases decrease, the amount of energy dispersed throughout a solution.

As a result of these effects, the entropy (ΔS) will be in either positive or negative. A positive value indicates that a favorable tendency towards greater dispersal of energy while a negative values represents more ordered systems. For example, the hydrophobic effect facilitates the release and further aggregation of hydrophobic residues as a result of protein folding. The amount of entropy in the system is initially increased as the protein unfolds but is quickly decreased as water molecules form clathrate structures around the exposed hydrophobic residues. This caged structure acts to control the random movement of the exposed protein while also providing the structural stability needed for the molecule to successfully transitions to a different structural state. However, as a result, the entropy becomes more positive. Although, this is not always the case. Other entropically favored effects, such as conformational entropy and the energy resulting from molecular vibrations, could become greater as a protein transitions its structure, and thus provide the solution with an overall negative entropy.

The analysis of thermodynamic parameters is complex because of the relationships they share with one another (Eq. 2 and Eq. 3). Using ITC, several thermodynamic parameters (K_B,

ΔG, ΔH, and ΔS) for a binding event can be obtained. The parameters will be affected by each source differently. Thus, analysis of all the parameters can give insight into each sources contribution to the overall thermodynamic driving force.

2.4 ITC Models

In order to properly analyze the ITC results, the data must be fit using computer software installed utilizing a variety of mathematical models. For the purposes of this thesis, The 7.0 origin software package supplied by MicroCal was used for fitting and analyzing the data obtained for this project [130].

The raw data obtained from an ITC experiment is opened using the downloaded software program, and further fit using a three step process. First, the software makes an initial estimate of n, K and ΔH based on the raw data. Then, mathematical binding models installed in the software are applied to the data and used to calculate the heat for each injection ($\Delta Q_{(i)}$). As a result, an improvement in the initial values of n, K, and ΔH are made using the Marquardt method [130]. This Origin® software uses a least square fit to minimize Chi squared (χ^2) in the fit of the heat flow per injection to an equilibrium binding equation. Included in the Origin® software are binding models applicable to a variety of binding interactions. The single site and sequential set of sites binding models will be discussed below.

2.4.1 Single Set of Sites

The binding of a ligand to a single set of identical sites on a macromolecule is represented by the following equilibrium expression, where K is the equilibrium or binding constant, Θ is the fraction of sites by which ligand X are occupied, and [X] is the concentration

of free ligand in solution.

$$K = \frac{\Theta}{(1-\Theta)[X]} \qquad \text{Eq. 4}$$

The total concentration of ligand, X_t, can be obtained using the equation below. The mathematical expression calculates X_t using the [X] and M_t parameters which were previously described.

$$X_t = [X] + n\Theta M_t \qquad \text{Eq. 5}$$

The total heat content, or Q, of the solution contained in V_o can be determined using equation 6. The variable V_o represents the solution at fractional saturation, Θ, and is determined relative to zero for the un-complexed species.

$$Q = n\Theta M_t \Delta H V_o \qquad \text{Eq. 6}$$

Equation 7 is further obtained by combined Eq. 5 and Eq. 6 and rearranging the resulting equation to equal 0.

$$\Theta^2 - \Theta\left[1 + \frac{X_t}{nM_t} + \frac{1}{nKM_t}\right] + \frac{X_t}{nM_t} = 0 \qquad \text{Eq. 7}$$

After solving for the fractional saturation variable, Θ, using equation 8, the resulting value can be entered into Eq. 7 to obtain equation 8. This mathematical formula can be used to find the overall $Q_{(i)}$ for the reaction.

$$Q_{(i)} = \frac{nM_t \Delta H V_o}{2}\left[1 + \frac{X_t}{nM_t} + \frac{1}{nKM_t} - \sqrt{\left(1 + \frac{X_t}{nM_t} + \frac{1}{nKM_t}\right)^2 - \frac{4X_t}{nM_t}}\right] \qquad \text{Eq. 8}$$

The previously calculated values of X_t, M_t, and V_o are entered into the curve fitting model prior to fitting the isotherm. However, the n, K, and ΔH in equation 8 are floating variables and may change as the curve is fit using the best binding curve parameters.

2.4.2 Sequential Sites

In a sequential set of sites binding model, only the total number of saturated sites can be determined. Therefore, the binding constants are obtained as the sites become progressively saturated and are thus defined relative to the progress of saturation. Equations 9a-c demonstrate the binding constant formula for a sequential set of sites with three successive binding events as represented by K_1, K_2, and K_3.

$$K_1 = \frac{[MX]}{[M][X]} \qquad K_2 = \frac{[MX_2]}{[MX][X]} \qquad K_3 = \frac{[MX_3]}{[MX_2][X]} \qquad \text{Eqs. 9a-c}$$

In the equation above, the concentrations of all complexed species $[MX_i]$ can be expressed in terms of [M].

The next set of equations uses the parameter, F_i, to represents the fractional amount of macromolecules in solution with i bound ligands.

$$F_o = \frac{1}{1 + K_1[X] + K_1K_2[X]^2 + K_1K_2K_3[X]^3} \qquad \text{Eq. 10}$$

$$F_1 = \frac{K_1[X]}{1 + K_1[X] + K_1K_2[X]^2 + K_1K_2K_3[X]^3} \qquad \text{Eq. 11}$$

$$F_2 = \frac{K_1 K_2 [X]^2}{1 + K_1[X] + K_1 K_2 [X]^2 + K_1 K_2 K_3 [X]^3} \quad \text{Eq. 12}$$

$$F_3 = \frac{K_1 K_2 K_3 [X]^3}{1 + K_1[X] + K_1 K_2 [X]^2 + K_1 K_2 K_3 [X]^3} \quad \text{Eq. 13}$$

For a sequential set of sites, the total concentration of ligand, X_t, can be obtained using equation 13 using the parameters [X] and M_t.

$$X_t = [X] + M_t \sum_{i=1}^{3} i F_i \quad \text{Eq. 14}$$

The binding curve for a set of sequential binding sites can be fit after obtaining the free ligand concentration [X] using the bisection numerical method from Eq. 14 through Eq. 13. These calculated values are further entered into the F_i equations in order to obtain $Q_{(i)}$ from the mathematical equation below.

$$Q_{(i)} = M_t V_o (F_1 \Delta H_1 + F_2[\Delta H_1 + \Delta H_2] + F_3[\Delta H_1 + \Delta H_2 + \Delta H_3] \quad \text{Eq. 15}$$

2.5 Circular Dichroism

Circular Dichroism (CD) spectroscopy serves as a valuable technique for evaluating the conformational changes in the secondary and tertiary structure of proteins and biomolecules. This technique works by measuring the difference in absorption between left-handed circularly polarized light and right-handed circularly polarized light of an optically active medium. Proteins and large biomolecules contain chiral chromophores which absorb circularly polarized light. The

amount of left or right handed circularly polarized light absorbed by these groups can vary depending on the conformation of the protein, which is easily affected by small environmental changes.

Therefore, CD spectroscopy serves as a useful tool to investigate the secondary structure of proteins and other biomolecules, both in their native state and when subjected to changes in environmental conditions, such as temperature, pH, or interactions with other molecules and ions. The data obtained from CD spectroscopy can be combined with other protein structural analysis methods such as X-ray crystallography or NMR to further evaluate or confirm the integrity of expressed domains of a multi-domain protein under normal and altered conditions.

2.5.1 Circular Dichroism Theory

The method behind CD spectroscopy is based on the differential absorption between left and right circularly polarized light. However, in order to understand how light is circularly polarized in CD for structural analysis, one must first understand the basics of polarization.

Light sources emit electromagnetic waves which are composed of oscillating electric and magnetic fields. These fields propagate perpendicularly to each other and to their direction of travel. When these fields oscillate in various directions, the light waves emitted are considered to be non-polarized. However, light can be polarized by manipulating the direction of the electric field vectors of a light wave. For example, linear polarized light is achieved when the electric fields are fixed to oscillate in a single plane concurrent with the direction of propagation. Circular polarized light, on the other hand, is a type of polarized light that results when the electric fields of a light wave are manipulated to propagate in a helical fashion around the axis of propagation. Two polarized light waves when combined, can also produce linear and circular

polarized light. Manipulating two polarized light waves to be in phase with each other at 90° will result in linearly polarized light, as shown in Figure 13 (AI) [133].

If one of the polarized light waves are positioned out of phase with the other by 45°, the resultant wave ceases to be linearly polarized and instead is projected as a helix. This helical shape of light is known as circularly polarized light (CPL) and propagates in either a right-handed (RCPL) or left-handed (LCPL) direction, see Figure 13 (AII).

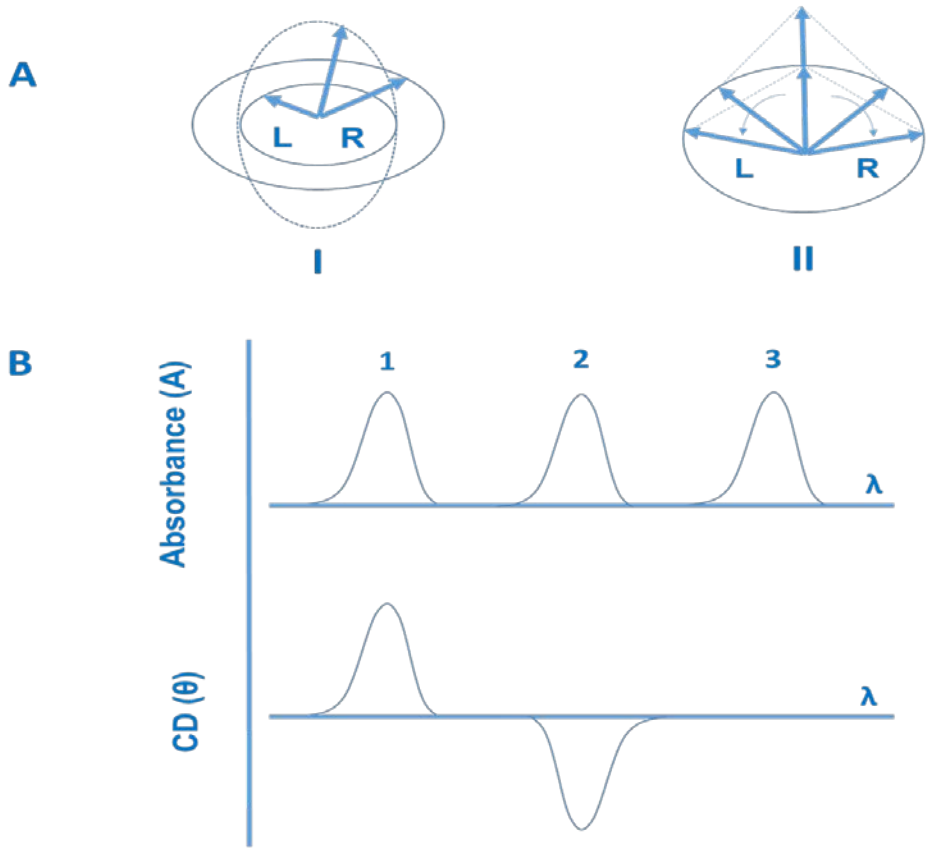

Figure 13. A schematic represention of circular polarized light. (A) A representation of circular polarized light when the components of plan polarized, left (L) and right (R) circular polarized light waves, are at equal (I) and unequal amplitudes (II). The resultant radiation is plane polarized light (I) and elliptically polarized light (II: dashed line), respectively. (B) The amount of L and R circularly polarized light absorbed by a sample determines the CD spectra produced, which depends on the secondary structure of the molecule in solution. A positive CD spectra is observed when more L (band 1) is absorbed. A negative CD spectra is obtained when more R (band 2) waves are absorbed. When equal amounts of L and R light are absorbed by a solution (ex. achiral solution), band 3, no CD spectra is observed. *Figure adapted from reference [133].*

RCPL and LCLP waves are non-superimposable; in other words, CPL is chiral. This characteristic means that right versus left CPL waves are, by definition, enantiomers and differ

from each other in how they interact with other enantiomeric species. Therefore, when an optically active solution is subjected to CPL, the RCPL and LCPL waves will interact differently with the chiral species of the sample. As a result, unequal amounts of RCPL and LCPL are absorbed by the molecules in solution. The difference in RCPL and LCPL can be measured and recorded as the ellipticity. This differential calculation mathematically defines circular dichroism.

2.5.2 Chiral Molecules

Samples containing chromophores are able to absorb light at different extents but are wavelength specific. A chromophore is referred to as a region or group within a molecule that will absorb electromagnetic energy within a particular wavelength range. However, in order to absorb CPL, a molecule of interest, subjected to the absorption wavelength range, must contain chromophoric regions or be present in an optically active asymmetric environment.

Due to the difference in absorption of a chromophoric solution, the resulting radiation will be detected as elliptical polarization. CD instruments (known as spectropolarimeters) measure the difference in absorbance between the L and R circularly polarized components (DA=ALAR). This difference can be converted to ellipticity (θ) in degrees, which is the common measurement reported in chemical CD studies.

2.6 Instrumentation

Circular dichroism spectroscopy measures the difference between right and left polarized light absorbed by a sample of interest. In order to obtain such measurements, CD spectroscopy utilizes a sophisticated spectrometry technique designed to manipulate monochromatic linearly

polarized light into circularly polarized light and further detect and plot the differential signal.

The general components of a CD spectrometer include: a high intensity light source, which usually emits light in the UV range (170-300 nm), a monochromator, a photo-elastic modulator (PEM), a lock-in amplifier, and a detector [133].

A CD spectrometer works by first initiating the light source located within the instrument to emit a stream of non-polarized light. This light is projected into the monochromator which polarizes the light into one wavelength specific for the sample. After leaving the monochromator, the linearly polarized light waves reach a photo elastic modulator (PEM) where it is further converted into left and right circularly polarized light waves.

The PEM is a specialized optical component known as a piezoelectric element. This element is cemented to a block of used silica that can oscillate at a resonance frequency, normally set at 50 kHz. When oscillating, the level of stress is induced upon the silica component which causes it to become birefringent [133]. The oscillating piezoelectric element induces alternating stress in the fused silica plate, thereby resulting in a dynamic quarter-wave plate.

The vertical component of the incoming linearly polarized light is slowed by a quarter-wave with respect to the horizontal component of the wave. The alternating silica plate then shifts to interact with the horizontal vectors, further slowing those light waves by a quarter degree respective to the vertical component of the polarized wave. The dynamic movement of the silica plate by a quarter wave produces left and right circularly polarized light that oscillates at the appropriate frequency. In order to successfully polarize the wavelength of light entering into the silica block, the amplitude of the oscillations can be changed. Light waves leaving the PEM are circularly polarized and will enter into the sample as equal amounts of left and right circularly polarized light. If no sample is present, equal amounts of RCPL and LCPL will result

in a linearly polarized light wave which the detector recognizes and reports as a steady signal on the output system. However, if an optically active sample is present, RCPL and LCPL will be absorbed in different amounts.

The resultant light that reaches the detector produces a signal that varies with PEM frequency [133]. A lock-in amplifier tuned to the PEM frequency measures the difference in intensity of the left and right components of the circularly polarized light. The average light intensity over time is measured as voltage direct current (vDC). This value is then used to scale the changes in CD measured by the voltage alternating current (vAC) signal [133]. The calculation used to obtain CD values, in units of millidegrees or change in absorbance, is demonstrate in equation 16. This value is obtained by dividing the vAC by the vDC signal followed by multiplication of the calibration factor (G).

$$CD = \frac{vAC}{vDC} * G \qquad \text{Eq. 16}$$

The obtained ellipticity or ΔA is plotted vs wavelength of light to give the observed CD spectra. It should be noted that in most biological studies, the observed CD signals are very small, i.e., ellipticities are typically in the range 10 millidegrees, corresponding to a difference in absorbance. It is therefore especially important in CD work to pay attention to the experimental conditions in order to ensure that meaningful data are obtained [133].

2.7 Protein Structure Identification

An advantage of the CD technique in studies of proteins is that complementary structural information can be obtained from a number of spectral regions [133].

Spectral bands are easily assigned to distinct structural features of a molecule. In proteins, the chromophores, which absorb light include: the peptide bond (240 nm), aromatic amino acid side

chains (260 to 320 nm), and disulfide bonds which produce a weak broad absorption bands (260 nm). Chromophores absorbing around 240 nm and below is principally due to the peptide bond. However, there is sometimes a weak but broad transition centered on 220 nm and a more intense transition around 190 nm that occurs when peptide bonds absorb light [134,135].

The conformational arrangement of some molecules does not always expose these chromophore regions which can alter the absorption pattern of the molecule. Larger molecules are composed of regular secondary structures, such as alpha helix, beta sheet, and random coils; these give rise to characteristic and identifiable CD spectra in the far UV (Figure 14). Therefore, these patterns are referenced when studying larger biomolecules using CD.

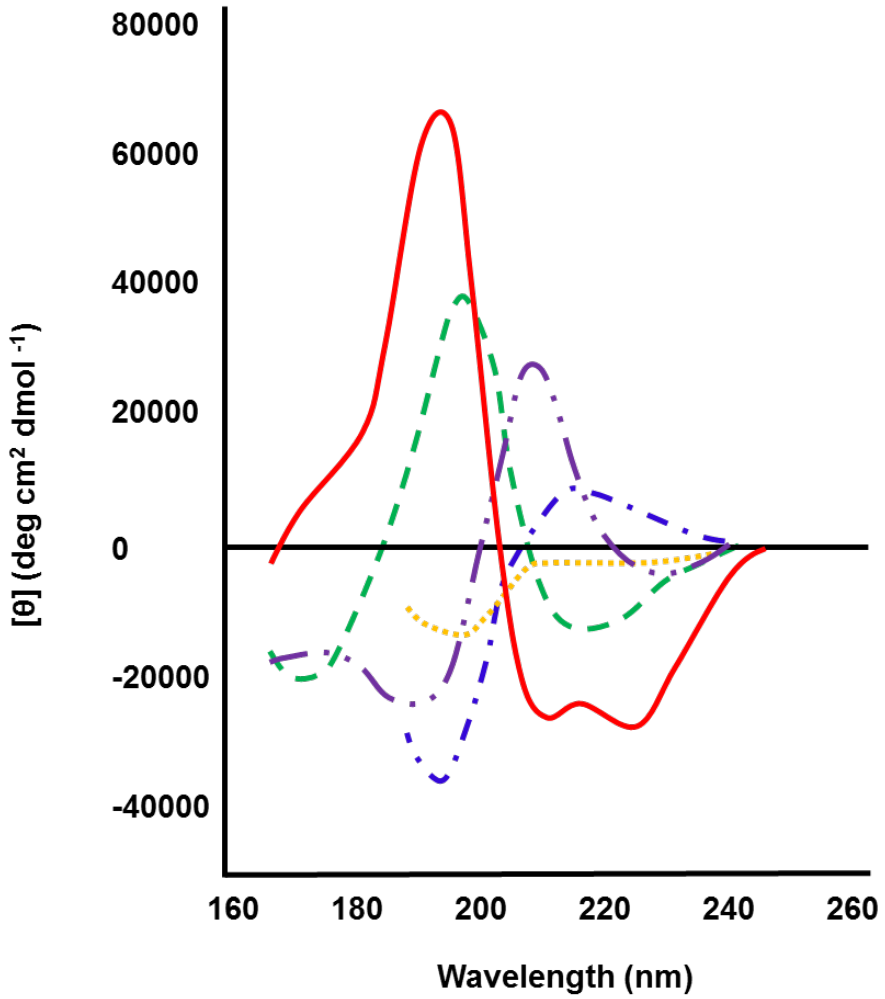

Figure 14. CD spectra representing the structural curves for protein solutions consisting of mostly alpha helices (—), anti-parallel beta sheets (— — —), type I beta-turn (—••—), extended alpha-helix or poly (Pro) II helix (—•—), or random coiled structures (•••). *Figure adapted from reference* [134].

Chapter 3: Cd^{2+} Binding to the Full Length HcTnC

Thermodynamic and CD spectroscopy studies were performed using purified full length HcTnC. The thermodynamics of cadmium binding to full length HcTnC were obtained and compared to the data from Ca^{2+} binding to full length HcTnC. Our studies provide binding affinities and stoichiometries of Cd^{2+} and Ca^{2+} binding to the protein and will allow us to determine if Cd^{2+} can displace Ca^{2+} under our conditions. This information may also infer where Cd^{2+} is binding on HcTnC, thereby providing preliminary information regarding possible mechanisms of cadmium toxicity at the molecular level. Previous studies have indicated that Cd^{2+} can bind to the EF II and the EF I loop of cTnC while NMR data suggest that Cd^{2+} binds to the C-domain of cTnC and induces structural transition similar to those observed when Ca^{2+} binds to the C-domain site of the protein. Through our experimental investigation of Cd^{2+} binding to full length cTnC we suggest that Cd^{2+} is binding to the C-domain and at a site other than EF II in the N domain. Our findings are presented and discussed below.

3.1 Experimental

The recombinant pET3d plasmid containing the gene for HcTnC was generously donated by the Chalovich lab at the Brody School of Medicine. The plasmid was expressed in the BL21(DE3) pLysS host strain of *Escherichia Coli*. The procedure used for protein expression and purification of full length HcTnC is described in Appendix A.

The Ca^{2+} and Cd^{2+} stock solutions for ITC and CD experimental analysis were prepared from atomic absorption standards purchased from Ricca chemicals. Metal stocks contained 5 mM calcium or cadmium, 50 mM Bis-Tris, 100 mM KCl at pH = 7.0 and were stored at room

temperature. In the preparation of all buffers, 18 MΩ water was used and reagents were purchased from Sigma-Aldrich as more than 99% pure unless otherwise mentioned.

3.2. Titrations of Ca^{2+} into full length HcTnC

Figure 15 shows a representative binding isotherm for the titration of Ca^{2+} ion into apo HcTnC. The thermogram displays two binding events at molar ratios of *n*=2 and *n*=3. The data presented in Figure 15 is very similar to data described by Skowronsky et al. but under different buffer conditions [132] and is therefore the second instance where binding of Ca^{2+} to the N-domain has been observed.

The first binding event at *n*=2 is highly exothermic and is represented by the negative peaks shown in the raw data of Figure 15 and by the negative enthalpic value (ΔH = -4.5 (± 0.1) kcal/mol) in Table 2. This binding event represents the first two Ca^{2+} ions binding to the protein. The tight inflection point and large K value of 5 (± 2) $\times 10^6$ obtained from fitting the data, is consistent with the binding of the structural Ca^{2+} ions to the C-domain of the protein. The second binding event at *n*=3 is endothermic and is represented by positive peaks in the raw data (top graph) of Figure 15, and by a positive change in enthalpy (ΔH = 1.3 (± 0.2) kcal/mol) in Table 2. The weak inflection and smaller K value of 5.0 (±0.4) $\times 10^4$ is consistent with the third Ca^{2+} ion binding to the regulatory or N-domain of HcTnC.

It is important to note that the K values observed are buffer and pH dependent values. Because Bis-Tris buffer binds to Ca^{2+} with a weak affinity [136], this must be taken into consideration in order to obtain buffer independent metal binding values. After adjusting for buffer according to previously published methods from our lab [132], the binding affinity associated with both the exothermic and endothermic events are 4 (± 2) $x10^7$ and 3.8 (± 0.3) $\times 10^5$

respectively (Table 2). These values are on the same order of magnitude as those previously reported in the literature [127].

Calcium ion binding to HcTnC occurs with positive cooperativity due to the hydrogen bond network located between EF-hand mates [34]. The data were therefore fit to a sequential binding model which assumes that binding of the first ligand or metal is followed by the second etc. Because the first and second Ca^{2+} ions bind in a single thermodynamic event, the binding parameters for these two ions were set equal to one another. The thermodynamic parameters obtained from fitting the data are listed in Table 2. Binding of the first two Ca^{2+} ions occur with a favorable Gibbs free energy (-9.0 ± 0.3 kcal/mol) and a favorable TΔS (4.5 ± 0.3 kcal/mol).

3.2.1 Thermodynamics of Ca^{2+} binding to C-domain of HcTnC

The binding of calcium to the C-domain is both enthalpically and entropically driven based on the respective negative ΔH and positive ΔS values shown in Table 2. These thermodynamic parameters are mostly a result of a series of interactions that occur within the protein as it transitions to a more folded structure upon binding calcium in the EF hand sites of the C-domain. Ca^{2+} binding to the C-domain of HcTnC induces a small structural shift in the protein which positions the amino acids, outside of the EF loop, closer together. This facilitates further electrostatic and hydrophobic interactions to occur within the protein structure, and as a result, a large amount of heat energy is produced. This heat energy not only gives an overall negative enthalpy, thereby making this event enthalpically favorable, but serves as the driving force in the transition of the protein from an unfolded to a more folded structure.

The interactions induced from calcium binding to the C-domain also increases the entropy of the system by releasing water molecules into the surrounding solvent. Clathrate water

molecules are usually found surrounding the hydrophobic residues in the C-domain of HcTnC. Calcium binding to the C-domain EF hand sites facilitates these non-polar amino acids to aggregate, which releases the bound water molecules into the solvent. As a result the entropy of the system is increased. Calcium binding through positive cooperativity to the C-domain also releases energy into the system, thereby, contributing to the overall favorable entropy value. The second loop of the C-domain has a more organized conformation as a result of the first Ca^{2+} binding. This puts a strain on the structure of the protein but is relieved when the second Ca^{2+} binds to the EF hand site. This interaction increases the degrees of freedom within the molecule and as a result, a larger amount of entropy is released into the system. Previous calorimetric studies have also shown that binding of Ca^{2+} to the C-domain of Bovine cTnC have also shown to be enthalpically and entropically favorable for similar reasons [34,127].

3.2.2 Thermodynamics of Ca^{2+} binding to the N-domain of HcTnC

Ca^{2+} binding to the N-domain occurs spontaneously with a ΔG of -6.4 (± 0.1) kcal/mol and is entropically driven based on both the positive ΔH of 1.3 (± 0.2) kcal/mol and ΔS of 7.7 (± 0.2) kcal/mol (Table 2). However, it is important to note that after accounting for the buffer contributions to binding, the enthalpy becomes negative [132], although not nearly as exothermic as the first binding event. This is because Ca^{2+} binding to the N-domain does not induce a conformational change that is as large as that observed in the C-domain. In fact, the NMR structures of both the apo and holo N-domain proteins are very similar [85,137]. Calcium binding to the regulatory domains of wheat germ calmodulin and skeletal troponin C at 25 °C and pH=7.0 have also been observed as entropically driven processes [138].

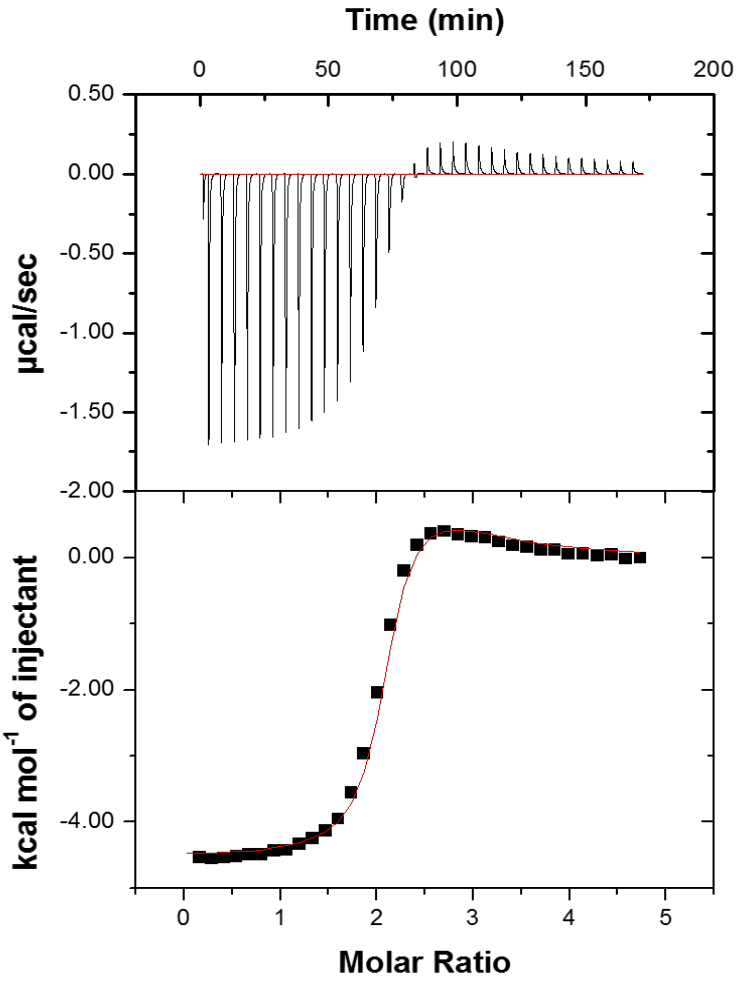

Figure 15. Representative ITC data of 1.5 mM Ca^{2+} titrated into 0.065 mM HcTnC. All samples are in 50 mM Bis-Tris (pH 7.0) and 100 mM KCl at 25 °C. Thermodynamic data are listed in Table 2.

Table 2. Best fit thermodynamic parameters and corrected values for Ca^{2+} binding to apo and Cd^{2+} saturated HcTnC. Thermodynamic values (ΔG, ΔH and ΔS) are reported in kcal/mol.

	Apo HcTnC	Corrected[a]	Cd^{2+} bound HcTnC	Corrected[a]
$K_{(1=2)}$	5 (± 2) $\times 10^6$	4 (± 2) $\times 10^7$	2 (± 1)$\times 10^4$	1 (± 1)$\times 10^5$
$\Delta G_{(1=2)}$	-9.0 (± 0.3)		-5.6 (± 0.5)	
$\Delta H_{(1=2)}$	-4.5 (± 0.1)		5 (± 3)	
$T\Delta S_{(1=2)}$	4.5 (± 0.3)		10.6 (± 3.0)	
K_3	5.0 (± 0.4) $\times 10^4$	3.8 (± 0.3) $\times 10^5$		
ΔG_3	-6.4 (± 0.1)			
ΔH_3	1.3 (± 0.2)			
$T\Delta S_3$	7.7 (± 0.2)			

a. Corrected K_b values are adjusted for buffer (Bis-Tris) at pH = 7.0 and ionic strength of 0.05 M.

3.2.3. CD Studies of Ca^{2+} binding to full length HcTnC

In addition to ITC, a study involving circular dichroism was performed to demonstrate the structural effects of calcium binding to HcTnC. The CD results in Figure 18 demonstrate that calcium binding to HcTnC produces a large molar ellipticity at 222 nm, which indicates an increase in alpha helical content of the protein. This is mostly due to the structural changes that occur in the C-domain when binding calcium as there is little change in structure in the N-domain upon Ca^{2+} binding as noted by NMR studies on the truncated form of the protein [85,137]. CD data obtained from skeletal TnC also support these findings, showing the majority of the 73% of structural changes occurring from Ca^{2+} binding to the C domain [139].

3.3 Thermodynamics of Ca^{2+} titrated into Cd^{2+} bound HcTnC

Figure 16 shows a representative thermogram for Ca^{2+} titrated into Cd^{2+} bound HcTnC after background subtraction. This single thermodynamic event is endothermic based on the

positive peaks shown in the isotherms of Figure 16 and the positive enthalpy values listed in Table 2. The isotherm also appears to represent one Ca^{2+} ion binding to protein. While it is not clear where the inflection occurs upon first inspection, fixing the n value to 1 in the fitting procedure yielded values with the least chi^2 and errors. The binding affinity for this event is 2 (± 1) $\times 10^4$ and 1 (± 1) $\times 10^5$ when corrected for buffer contributions.

The interaction between Ca^{2+} and Cd^{2+} bound HcTnC is spontaneous and occurs with a ΔG = -5.6 (± 0.5) kcal/mol. The positive ΔH and ΔS values of 5 (± 3) and 10.6 (± 3.0) kcal/mol as listed in Table 2 indicate that Ca^{2+} binding under such conditions is an entropically driven process. This is similar to the binding of Ca^{2+} to apo N-domain of HcTnC (ΔG = -5.6 kcal/mol0 with the enthalpy and entropy of Ca^{2+} binding in this case being more positive by 3.7 and 2.9 kcal/mol respectively.

Although ITC studies alone cannot determine where the calcium ion is binding, the very similar ΔG's of calcium binding between apo and cadmium bound protein ($\Delta\Delta G = \left| 0.8 \right.$ kcal/mol $\left.\right|$) indicate that Ca^{2+} is capable of binding to the N-domain of HcTnC even in the presence of Cd^{2+}. The different ΔS and ΔH values suggest that Cd^{2+} has altered the binding of Ca^{2+} to the protein. CD studies suggest the presence of Cd^{2+} alters the structure of the Ca^{2+} bound protein slightly (see below) which may explain the differences observed in ΔH and ΔS. More studies need to be done to determine if cadmium has an effect on the interaction of HcTnC with other troponin proteins.

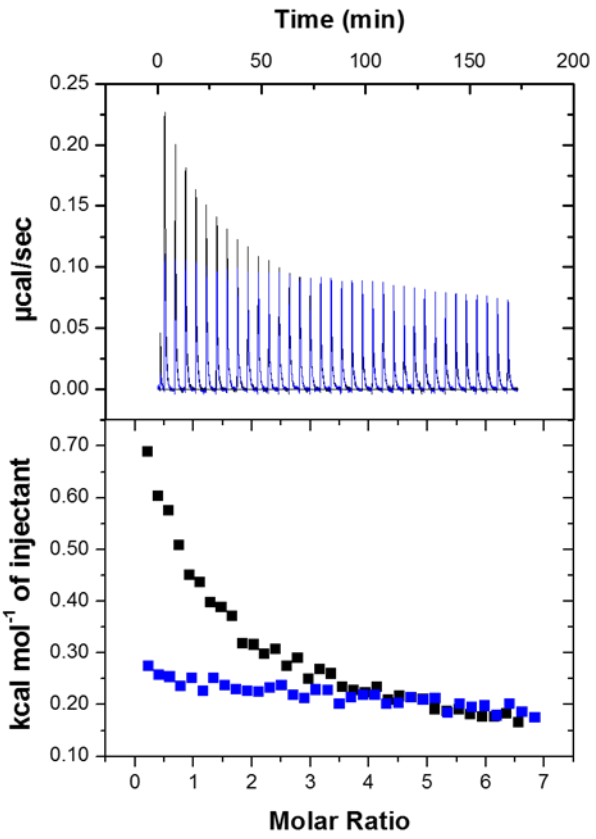

Figure 16. Representative ITC data of 1.5 mM Ca^{2+} titrated into 0.047 mM HcTnC containing 0.27 mM Cd^{2+}. The blue line represents the Ca^{2+} into buffer plus Cd^{2+} (0.27 mM) background. All samples are in 50 mM Bis-Tris (pH 7.0) and 100 mM KCl at 25 ˚C. Thermodynamic data are listed in Table 3.

3.4 Thermodynamics of Cd^{2+} titrated into apo HcTnC

The isotherm in Figure 17a represents the titration of Cd^{2+} into apo HcTnC. The data appear to consist of one thermodynamic event, but is best fit to a "sequential set of sites" model that accounts for three Cd^{2+} ions binding to the protein. The first event observed in Figure 17a is exothermic and is represented by negative peaks in the raw data (top graph) of Figure 17a and by

the negative enthalpy values listed in Table 3. The first event is shown by a sharp inflection at molar ratio of *n*=2 which indicates that two Cd^{2+} ions are binding for every one mol of apo HcTnC.

The binding parameters for both Cd^{2+} ions cannot be resolved in the data and are therefore are represented by a single binding affinity of 1.6 (± 0.1) $\times 10^8$ and an enthalpy of -13.7 (± 0.1) kcal/mol. The Gibbs free energy for the first two Cd^{2+} ions binding to the protein is energetically favorable with a $\Delta G_{1=2}$ equal to -9.8 (± 0.1) kcal/mol. This process is enthalpically driven, as the TΔS is negative kcal/mol and not favorable and is analogous to two Ca^{2+} ions binding to the C-domain of the protein.

Our data do not indicate where these Cd^{2+} ions are binding, however previous ^1H NMR studies reveal that the addition of two equivalents of Cd^{2+} to bovine cardiac TnC produces a spectrum that is identical to that obtained when two equivalents of Ca^{2+} are added to the protein [140] thus suggesting that binding is occurring to the Ca^{2+} binding loops of the C-domain. In addition, ^{113}Cd NMR experiments reveal that the two cadmium equivalents bind with very high affinity and that just as in the case of Ca^{2+} binding to the C-domain of HcTnC, these two Cd^{2+} ions are thought to bind with positive cooperativity. NMR structures of full length skeletal HcTnC also reveal the presence of two Cd^{2+} ions bound to the C-domain of the protein only [56]. Taken together, we believe the two high affinity Cd^{2+} ions seen in our ITC data are binding to the C-domain of HcTnC, displaying a single thermodynamic event consistent with two Cd^{2+} ions binding with one K_a and heat exchange of ΔH1 + ΔH2. These Cd^{2+} ions bind an order of magnitude more tightly than Ca^{2+} and are capable of competing with Ca^{2+} for these two sites.

The second binding event represents a third Cd^{2+} ion binding to apo HcTnC. This thermodynamic event is exothermic and is depicted by small negative peaks located close to the

baseline in the raw data of Figure 17a and by the negative enthalpy values obtained in Table 3. The binding affinity for the binding of the third Cd^{2+} is 4 (± 3) $\times 10^5$ and has an enthalpy of -1.3 kcal/mol. This event is also spontaneous, occurring with a ΔG of -6.2 (±0.4) kcal/mol and a very favorable ΔS (4.9 kcal/mol).

Recent crystal structures of Cd^{2+} bound to the regulatory domain of HcTnC in the presence and absence of deoxycholate [32,33] did show Cd^{2+} ion binding to both EF hand loops I and II. We believe that the second binding and much weaker binding event corresponds to the third Cd^{2+} ion. Because Ca^{2+} appears to bind to loop II in the Cd^{2+} saturated state with similar Gibbs free energy as the apo scenario, we propose that the third Cd^{2+} ion observed in our ITC thermogram is possibly binding to the defunct EF hand (loop I).

While previous ^{1}H-NMR studies comparing Ca^{2+} and Cd^{2+} binding to bovine cTnC did display slight differences in spectra after the addition of 3 equivalents of metal, ^{113}Cd NMR could not detect the binding of the third ion. If bound to the defunct loop, Cd^{2+} forms a thiolate bond with the cysteine residue present in the loop. The resonance signature for this thiolate bond in ^{113}Cd would be present at ~600 ppm and would be difficult to detect without ^{113}Cd enrichment. Although more studies are necessary, our current model based on the current thermodynamic study is that Cd^{2+} is binding to the defunct loop of HcTnC.

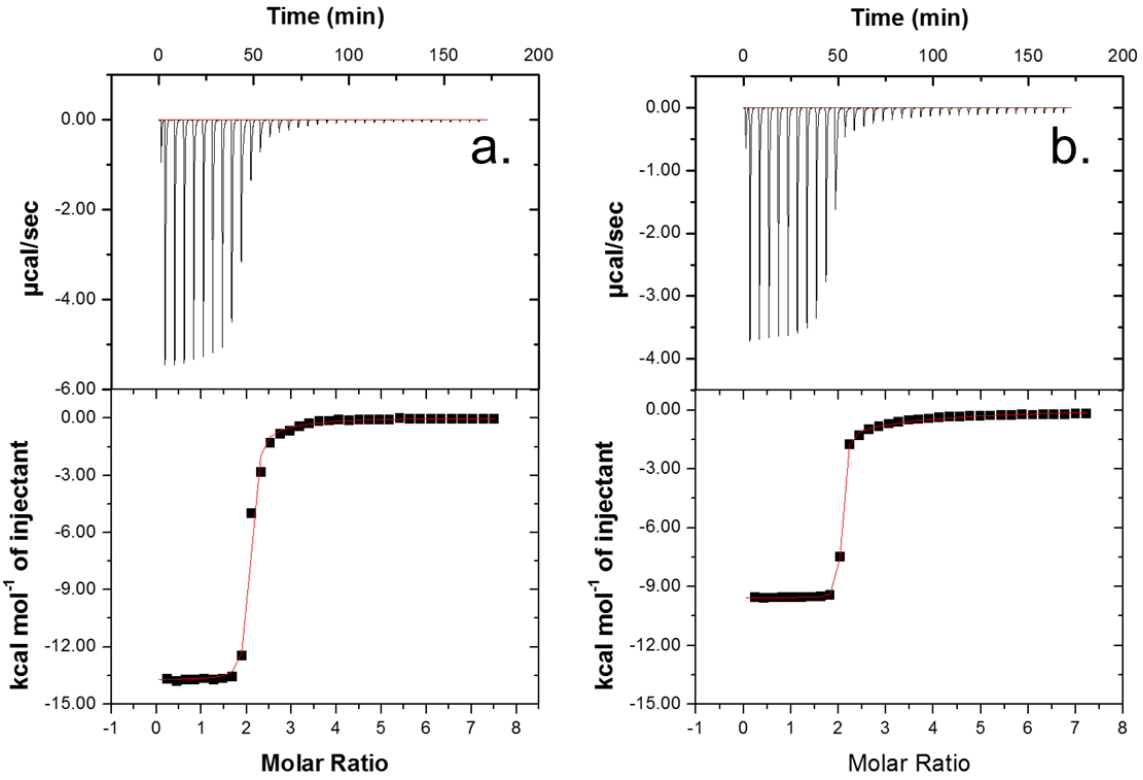

Figure 17. Representative ITC data of (a) 1.5 mM Cd^{2+} titrated into 0.041 mM apo HcTnC and (b) 1.5 mM Cd^{2+} titrated into 0.043 mM HcTnC containing 0.27 mM Ca^{2+}. All samples are in 50 mM Bis-Tris (pH 7.0) and 100 mM KCl at 25 ˚C. Thermodynamic data are listed in Table 3.

Table 3. Best fit thermodynamic parameters for Cd^{2+} binding to apo and Ca^{2+} bound HcTnC. Thermodynamic values (ΔG, ΔH and ΔS) are reported in kcal/mol.

	Apo HcTnC	Corrected[a]	Ca^{2+} bound HcTnC	Corrected[b]
$K_{1=2}$	2.0 (± 0.1)×10^7	1.6 (± 0.1)×10^8	3 (± 1)×10^7	3 (± 1)×10^8
$\Delta G_{1=2}$	-9.8 (± 0.1)		-10.1 (± 0.2)	
$\Delta H_{1=2}$	-13.7 (± 0.1)		-9.1 (± 0.7)	
$T\Delta S_{1=2}$	-3.9 (± 0.1)		1.0 (± 0.3)	
K_3	4 (± 3)×10^4	4 (± 3)×10^5	1.3 (± 0.2)×10^4	1.4 (± 0.2)×10^5
ΔG_3	-6.2 (± 0.4)		-6.0 (± 0.2)	
ΔH_3	-1.3 (± 0.2)		-3.1 (± 0.5)	
$T\Delta S_3$	4.9 (± 0.4)		-2.9 (± 0.5)	

a. Corrected K_b values are adjusted for buffer (Bis-Tris) at pH = 7.0 and ionic strength of 0.1 M.

3.5. Thermodynamics of Cd^{2+} binding to Ca^{2+} saturated HcTnC

Figure 17b is a representative thermogram of Cd^{2+} titrated into Ca^{2+} saturated HcTnC. The thermogram is very similar to Cd^{2+} titrated into apo protein with two ions binding in a single exothermic event at n=2 and a subsequent exothermic event at n=3. The data were best fit to a "set of sequential sites" model with n=3 sites. The binding affinity for the first event is 3 (±1) x 10^7 which is within error of the first two Cd^{2+} ions binding to apo HcTnC. The ΔG of this event is -10.1 kcal/mol and occurs spontaneously as a result of enthalpically and entropically favored events. While the overall Gibbs free energy is similar to the apo scenario, closer inspection of the enthalpy and entropy of binding reveals key differences. The enthalpy of Cd^{2+} binding has become more disfavored by 4.6 kcal/mol while the entropy has compensated by becoming more favored by 4.9 kcal/mol.

A comparison of the binding constants obtained from the Ca^{2+} and Cd^{2+} binding to apo HcTnC reveal that Cd^{2+} binding is an order of magnitude larger than Ca^{2+}. This indicates that Cd^{2+} is capable of displacing the first two Ca^{2+} ions from the protein. A simple displacement model using the following equation, $K_{Cd\ apparent} = K_{Cd}/(K_{ca} \times [Ca])$, suggests that this displacement would occur with an apparent binding constant of ~4×10^3. This is not observed in our thermodynamic titration therefore indicating that metal displacement is occurring via a different mechanism. It is important to note that the first two Ca^{2+} ions bind with positive cooperativity where the first Ca^{2+} ion triggers a structural change that allows the second metal ion to bind with a much higher affinity. The result is that both ions saturate with a single K_a value and heat exchange of $\Delta H1 + \Delta H2$. In terms of displacement, the first Cd^{2+} ion displaces the more weakly bound Ca^{2+} ion (the first Ca^{2+} to bind the protein). To better describe our thermodynamics, we believe that the binding of the first Cd^{2+} ion to Ca^{2+} ion site 1 weakens the binding of the second Ca^{2+} thereby allowing the second Cd^{2+} to bind to the protein with a high affinity. The result is that the two Cd^{2+} ions bind to the protein with a single thermodynamic event, with K_a's similar to the apo scenario, and a heat exchange of $\Delta H1 + \Delta H2$.

The second thermodynamic event is exothermic and is depicted by small negative peaks located close to the baseline in the raw data of both isotherms in Figure 17 and by the negative enthalpy values obtained during each titration. The binding affinity of $1.4 (\pm 0.2) \times 10^5$ represents the third Cd^{2+} ion binding to calcium saturated HcTnC and is similar to the apo scenario with a Gibbs free energy of -6.0 (±0.2) kcal/mol. Again the enthalpy and entropy of binding is different with the enthalpy becoming disfavored by 1.8 kcal/mol and the entropy becoming more favored by 7.8 kcal/mol. If the third Cd^{2+} is binding to the defunct loop, our data

suggests that Ca^{2+} present in the functional loop does not have a major impact on the overall Gibbs free energy but does effect the enthalpy and entropy slightly.

3.6. CD studies of Ca^{2+}, Cd^{2+}, and Ca^{2+}/Cd^{2+} bound HcTnC

The CD spectra of apo, Ca^{2+}, Cd^{2+}, and Ca^{2+}/Cd^{2+} bound HcTnC are displayed in Figure 18. Notable differences are apparent when comparing representative CD spectra of apo HcTnC to the Ca^{2+} and Cd^{2+} bound forms. The graphs show that both Ca^{2+} and Cd^{2+} ions are capable of inducing secondary structural changes upon binding albeit with a few differences. It is important to note that these differences are not due to simple concentration differences as they cannot be explained by scaling of the spectra. These changes are most notable at 209 and 222 nm, the spectral region that corresponds to alpha-helical structure, and are most dramatic for Ca^{2+} ion binding. This spectral changes are more dramatic for Ca^{2+} than Cd^{2+} ion and as discussed previously, these large changes in ellipticity are due to structural changes that occur in the C-domain as a result of metal ion binding [139]. The large changes in ellipticity observed upon Cd^{2+} binding provide further support that cadmium is indeed binding to the C-domain.

Even more interesting, the spectrum representing the mixed metal species (Ca^{2+}/Cd^{2+}) resembles that of the Ca^{2+} bound protein with a minor difference in ellipticity centered at 220 nm. This indicates that the structure obtained from Cd^{2+} binding to apo protein is very different from the structure obtained when Cd^{2+} displaces Ca^{2+} from the protein and can perhaps be explained by a model that invokes metal ion cooperativity (see discussion above).

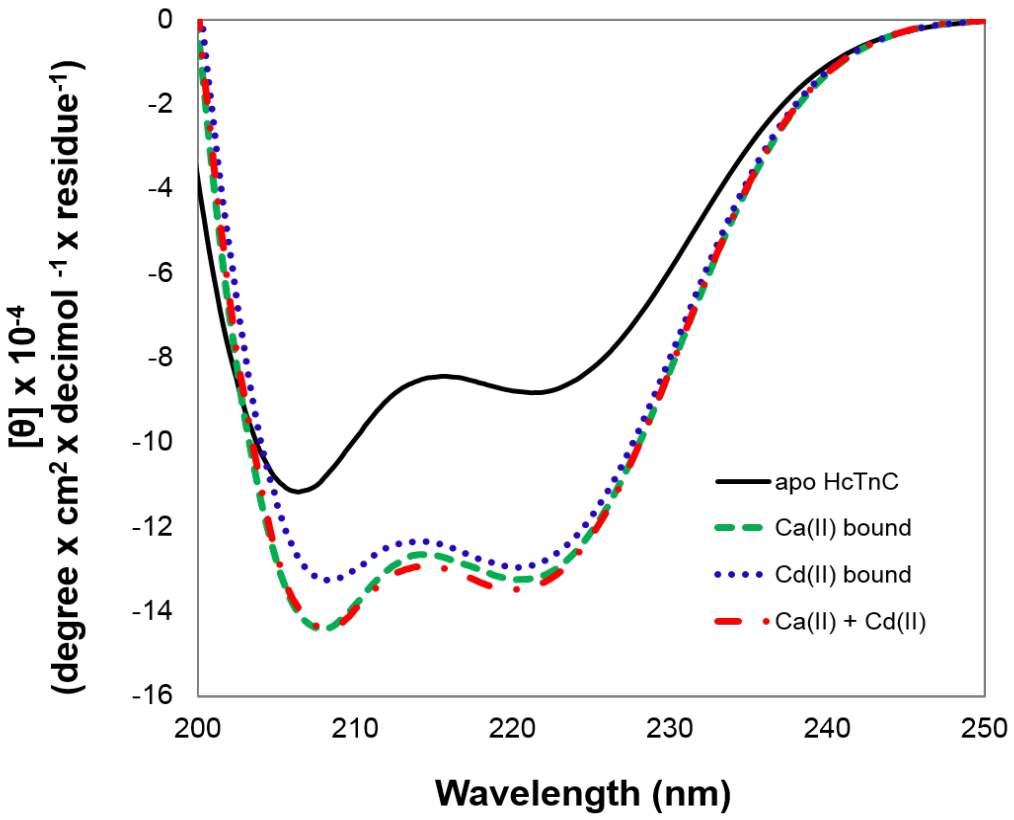

Figure 18. Circular dichroism data of (▬) 0.02 mM apo HcTnC, (▬ ▬) 2 mM Ca^{2+} plus 0.02 HcTnC, (• • •) 2 mM Cd^{2+} plus 0.02 mM HcTnC, and (▬ •) 2 mM Ca^{2+} and 2 mM Cd^{2+} plus 0.02 mM $HcTnC_{1-89}$**.** All samples are in 10 mM Bis-Tris (pH 7.0) and 10 mM KCl. Data were collected at 25 ˚C.

3.7 Conclusions

In conclusion, our thermodynamic studies indicate that a total of three Cd^{2+} ions bind to HcTnC. The first two high affinity Cd^{2+} ions appear to bind to the protein with a single thermodynamic event and binding affinity that is an order of magnitude larger than Ca^{2+}. Previous studies probing Cd^{2+} ion binding to bovine cTnC using ^{1}H and ^{113}CD NMR suggest that both Cd^{2+} ions bind to the C-domain. This is supported by our CD studies which show large structural changes indicative of metal ion structural reorganization to the C-domain.

The third Cd^{2+} ion binds to the protein with an affinity that is ~2 orders of magnitude smaller than the high affinity metal ions. While previous NMR structures demonstrate the ability of Cd^{2+} to bind to both EF hand loops I and II, our studies suggest that Cd^{2+} has a preference for loop I (the defunct loop) under our conditions. More specifically, our ITC studies show that Ca^{2+} ion binding to HcTnC in the presence of Cd^{2+} occurs with a Gibbs free energy that is similar to the binding of Ca^{2+} to the N-domain. In addition, the third Cd^{2+} ion binds to the apo protein with a Gibbs free energy that is similar to binding in the presence of Ca^{2+} thus indicating that both ions bind to different loops in the protein. The slight differences in enthalpy and entropy indicate that the presence of metal at one site alters the structure or conformation of metal at the other site thus indicating communication between the two EF hands.

Chapter 4: Cd^{2+} Binding to the N-Domain of HcTnC

A recent crystal structure reported several Cd^{2+} ions binding to the regulatory domain of HcTnC ($HcTnC_{1-89}$). Two of these ions were located in EF hands I and II and with geometries similar to Ca^{2+}. In this study, we utilized ITC and CD to characterize the thermodynamics and structures of Cd^{2+} binding to the isolated N domain of HcTnC ($HcTnC_{1-89}$) under our buffering conditions in order to provide more information regarding the location of Cd^{2+} binding to the protein. To our surprise, ITC data yielded slightly unexpected results and data was best fit to a model suggesting the binding of four Cd^{2+} ions. Data is presented below in addition to a discussion regarding the putative binding sites for each Cd^{2+} ion.

4.1 Experimental

Thermodynamic and CD spectroscopy studies were performed using the purified N-domain of HcTnC ($HcTnC_{1-89}$). The recombinant pET3d plasmid containing the gene for $HcTnC_{1-89}$ was generously donated by the Chalovich lab at the Brody School of Medicine. The plasmid was expressed in the BL21(DE3) pLysS host strain of *Escherichia Coli*. The procedure used for protein expression and purification of $HcTnC_{1-89}$ is described In Appendix A.

The Ca^{2+} and Cd^{2+} stock solutions for ITC and CD experimental analysis were prepared from atomic absorption standards purchased from Ricca chemicals. Metal stocks contained 5 mM calcium or cadmium, 50 mM Bis-Tris, 100 mM KCl at pH = 7.0 and were stored at room temperature. In the preparation of all buffers, 18 MΩ water was used and reagents were purchased from Sigma-Aldrich as more than 99% pure unless otherwise mentioned.

4.2 Thermodynamics of Ca^{2+} binding to apo and Cd^{2+} bound $HcTnC_{1-89}$

Figures 19a and 19b represent Ca^{2+} binding to both apo and Cd^{2+} bound $HcTnC_{1-89}$ respectively. Both thermograms in Figure 19 display a single endothermic binding event but with a several noticeable differences. First, the thermogram in Figure 19 displays a modest inflection at n=1 that is slightly sigmoidal in shape whereas the inflection in Figure 19b is less distinctive. Second, the titration of Ca^{2+} into apo protein reaches equilibrium after the addition of 4 equivalents of Ca^{2+} whereas Ca^{2+} titrated into Cd^{2+} bound protein is shown to reach equilibrium after 40 equivalents of Ca^{2+} has been added. This suggests that binding of Ca^{2+} to the apo protein is stronger than that of Cd^{2+} bound $HcTnC_{1-89}$. This is further supported by the conditional binding constants (K) listed in Table 4 where K for Ca^{2+} binding to the apo protein (3.8×10^4) is an order of magnitude larger than Ca^{2+} binding to Cd^{2+} bound $HcTnC_{1-89}$ (2.3×10^3).

The most important differences lie in the thermodynamic parameters noted in Table 4. The Gibbs free energy for Ca^{2+} binding to apo $HcTnC_{1-89}$ is more favorable by 1.6 kcal/mol while the enthalpy of Ca^{2+} binding to apo protein is more favorable by 9.3 kcal/mol. While both binding scenarios are entropically favored, the $T\Delta S$ for Ca^{2+} binding to Cd^{2+} bound protein is more favorable suggesting that binding occurs with either more conformational flexibility or release of solvent into the bulk solution.

These differences suggest that the binding interaction between Ca^{2+} and $HcTnC_{1-89}$ is weakened in the presence of cadmium ion. Either both calcium and cadmium ions are competing for the same binding site in the protein and Ca^{2+} is displacing Cd^{2+} thereby resulting in different thermodynamic parameters, or the cadmium ion could be interacting with the protein at an alternate site which could alter Ca^{2+} binding to the protein in loop II. As was discussed in

Chapter 3, Ca^{2+} and Cd^{2+} binding studies to full length HcTnC support the second scenario where Ca^{2+} binds to loop II and Cd^{2+} appears to bind to perhaps loop I in the N-domain. Therefore the presence of Cd^{2+} to loop I may alter the structure and binding of Ca^{2+} to loop II thereby resulting in a less favorable enthalpy and Gibbs free energy.

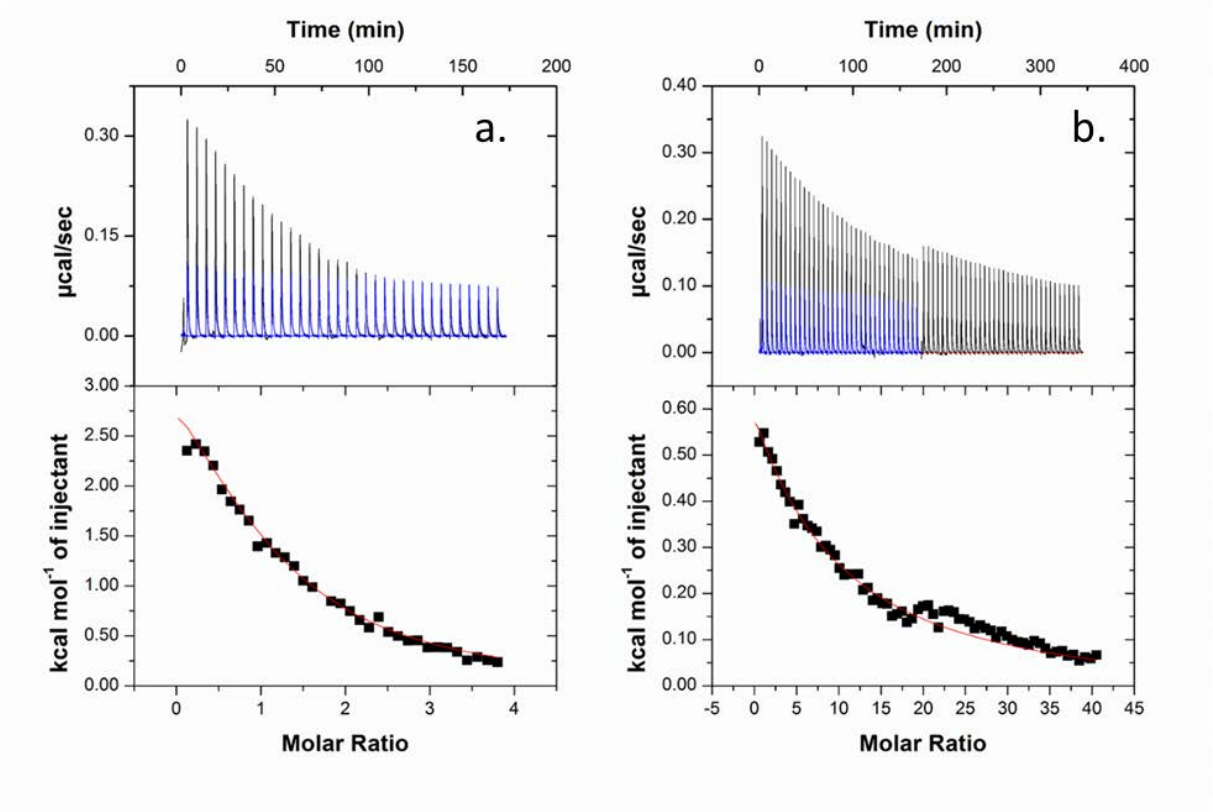

Figure 19. Representative ITC data of (a) 0.5 mM Ca^{2+} titrated into 0.027 mM $HcTnC_{1-89}$ and (b) 2.0 mM Ca^{2+} titrated into 0.022 mM $HcTnC_{1-89}$ containing 0.25 mM Cd^{2+}. All samples are in 50 mM Bis-Tris (pH 7.0) and 100 mM KCl at 25 ˚C. Thermodynamic data are listed in Table 4.

Table 4. Best fit thermodynamic parameters and corrected values for Ca^{2+} binding to apo and Cd^{2+} bound $HcTnC_{1-89}$. Thermodynamic values (ΔG, ΔH and ΔS) are reported in kcal/mol.

	Apo $HcTnC_{1-89}$	Corrected[a]	Cd^{2+} bound $HcTnC_{1-89}$	Corrected[a]
n	0.98 (± 0.3)		fixed	
K	3.8 (± 0.3) $\times 10^4$	2.9 (± 0.2) $\times 10^5$	2.3 (± 0.6)$\times 10^3$	1.7 (± 0.5) $\times 10^4$
ΔG	-6.2 (± 0.1)		-4.6 (± 0.2)	
ΔH	5.5 (± 0.5)		14.8 (± 0.1)	
$T\Delta S$	11.7 (± 0.5)		19.4 (± 0.2)	

a. Corrected K_b values are adjusted for buffer (Bis-Tris) at pH=7.0 and ionic strength of 0.1 M.

4.3 Thermodynamics of Cd^{2+} binding to apo $HcTnC_{1-89}$

Cd^{2+} binding to apo $HcTnC_{1-89}$ displays 3 distinct thermodynamic events (Figure 20a) in contrast to a single event seen for Ca^{2+} binding to apo protein. The first exothermic event occurs at a molar ratio of n=1 which is immediately followed by a second more exothermic event at n=2. Both events have steep slopes associated with them indicating strong binding. The third event is slightly less exothermic and shows slight sigmoidal behavior and a weak inflection at n= 4 thus indicating weaker binding. Data were best fit to a "sequential set of sites model" with the number of sites set to 4. Because it is difficult to distinguish binding of the third and fourth Cd^{2+} ion, parameters (K and H) were set equal to one another. The conditional binding constants in addition to remaining thermodynamic parameters are listed in Table 5.

Each binding event is spontaneous as represented by the negative Gibbs free energy values of -10.0 (± 0.1) kcal/mol, -9.1 (± 0.1) kcal/mol and -6.1 (± 0.1) kcal/mol for Cd^{2+} ions 1, 2, and 3=4 respectively. The enthalpies are all exothermic and favorable as represented by the

respective ΔH values -7.3 (± 0.3) kcal/mol, -8.2 (± 0.6) kcal/mol, -9.0 (± 0.9) kcal/mol. A positive and favorable entropy is associated with the first two binding events followed by a negative an unfavorable entropy for the third binding event. The entropy values are reported as 2.7 (± 0.3) kcal/mol, 0.9 (± 0.6) kcal/mol, -2.9 (± 0.9) kcal/mol in Table 5 for each respective binding event.

The two high affinity cadmium ions clearly bind more tightly than Ca^{2+} under the conditions studied. When correcting for buffers (Table 4 and 5), the tightest bound cadmium ion has a K_a that is 3 orders of magnitude greater than Ca^{2+}. Although Ca^{2+} may be able to compete with the third or fourth Cd^{2+} ion, it is clearly not capable of displacing the first two cadmium ions.

4.4 The thermodynamics of Cd^{2+} binding to Ca^{2+} bound $HcTnC_{1-89}$

Cd^{2+} ion binding to Ca^{2+}saturated protein (Figure 20b) displays only two exothermic events as opposed to three observed in the apo scenario. The first thermodynamic event occurs at an n=2 while the second occurs at n=4. The first two sites are now indistinguishable and the data were fit to a "sequential set of binding sites" with sites 1=2 and 3= 4 respectively. All thermodynamic parameters can be found in Table 5. The conditional binding constant for both sites 1 and 2 was found to be 7 (± 1) $\times 10^6$, which is within error to the second binding constant reported for Cd^{2+} binding to apo protein. This suggests that calcium present in the protein has weakened the binding of the first Cd^{2+} by an order of magnitude. The enthalpy of the first two cadmium ions binding to the protein is -9.0 (± 0.2) kcal/mol, which is 0.8 kcal/mol more favorable than the second Cd^{2+} binding to the apo protein. This suggests that calcium present in

the protein has also weakened binding to EF hand loop I and both Cd^{2+} ions are now binding with an average enthalpy of -9.0 kcal/mol.

While there are clear changes in the binding of the first two cadmium ions to the protein, the thermodynamic parameters for the third and fourth metal ions have not changed and all parameters reported are within error (Table 5). This suggests that Ca^{2+} present in the truncated protein does not alter Cd^{2+} binding to these sites.

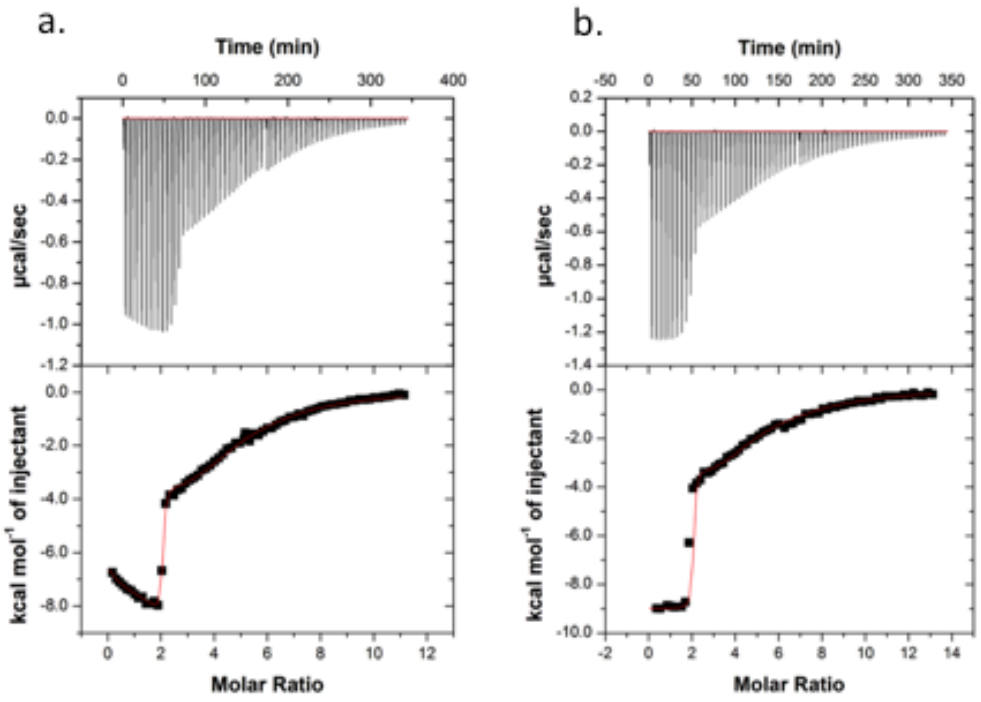

Figure 20. Representative ITC data of (a) 0.5 mM Cd^{2+} titrated into 0.017 mM apo $HcTnC_{1\text{-}89}$ and (b) 0.5 mM Cd^{2+} titrated into 0.016 mM $HcTnC_{1\text{-}89}$ containing 0.125 mM Ca^{2+}. All samples are in 50 mM Bis-Tris (pH 7.0) and 100 mM KCl at 25 ˚C. Thermodynamic data are listed in Table 5.

Table 5. Best fit thermodynamic parameters for Cd^{2+} binding to apo and $Ca2^{+}$ bound $HcTnC_{1\text{-}89}$. Thermodynamic values (ΔG, ΔH and ΔS) are reported in kcal/mol.

	Apo $HcTnC_{1\text{-}89}$	Corrected[a]	Ca^{2+} bound $HcTnC_{1\text{-}89}$	Corrected[a]
K_1	2.1 (± 0.3)×10^7	2.2 (± 0.3)×10^8	--	--
ΔG_1	-10.0 (± 0.1)	--	--	--
ΔH_1	-7.3 (± 0.3)	--	--	--
$T\Delta S_1$	2.7 (± 0.3)	--	--	--
K_2 (β_2)	5 (± 1)×10^6	5 (± 1)×10^7	7 (± 1)×10^6 [b]	8 (± 1)×10^7
ΔG_2	-9.1 (± 0.2)	--	-9.4 (± 0.1)	--
ΔH_2	-8.2 (± 0.2)	--	-9.0 (± 0.2)	--
$T\Delta S_2$	0.9 (± 0.3)	--	0.4 (± 0.2)	--
$K_{3,4}$ ($\beta_{3.4}$)	3 (± 1)×10^4	3 (± 1)×10^5	2.7 (± 0.4)×10^4	2.9 (± 0.4)×10^5
$\Delta G_{3,4}$	-6.1 (± 0.1)	--	-6.0 (± 0.1)	--
$\Delta H_{3,4}$	-9.5 (± 0.5)	--	-9.4 (± 0.3)	--
$T\Delta S_{3,4}$	-3.4 (± 0.5)	--	-3.4 (± 0.3)	--

a. Corrected K_b values are adjusted for buffer (Bis-Tris) at pH=7.0 and ionic strength of 100 mM.

b. Sites 1 and 2 cannot be distinguished and either represent a β value or metals binding with the same affinity.

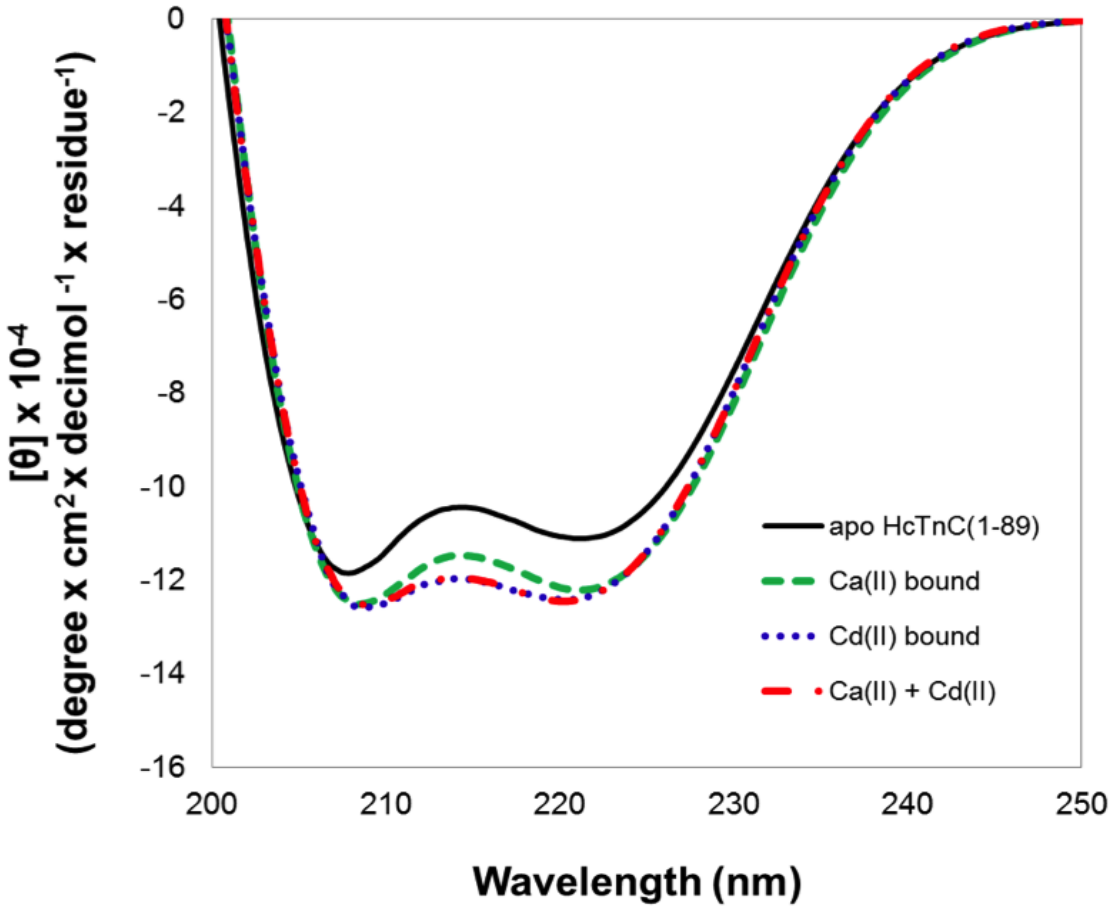

Figure 21. Circular dichroism data of (▬) 0.02 mM apo $HcTnC_{1\text{-}89}$, (▬ ▬) 2 mM Ca^{2+} plus 0.02 $HcTnC_{1\text{-}89}$, (• • •) 2 mM Cd^{2+} plus 0.02 mM $HcTnC_{1\text{-}89}$, and (▬ •) 2 mM Ca^{2+} and 2 mM Cd^{2+} plus 0.02 mM $HcTnC_{1\text{-}89}$. All samples are in 10 mM Bis-Tris (pH 7.0) and 10 mM KCl. Data were collected at 25 ˚C.

4.4 Circular dichroism of Ca^{2+}, Cd^{2+}, and Ca^{2+}/Cd^{2+} bound to $HcTnC_{1-89}$

Figure 21 displays representative CD spectra of apo $HcTnC_{1-89}$, Ca^{2+} bound $HcTnC_{1-89}$, Cd^{2+} bound $HcTnC_{1-89}$, and Ca^{2+}/Cd^{2+} bound $HcTnC_{1-89}$. There is a notable increase in ellipticity observed between 210 and 220 nm upon addition of Ca^{2+} to apo-HcTnC. These changes are very small and therefor suggest minute structural difference between apo and metal bound species. This is further supported by the very small differences in the NMR structures of apo and Ca^{2+} bound $HcTnC_{1-89}$ [85,100,137]. There is a slight difference in CD signal between the Ca^{2+} and Cd^{2+} bound $HcTnC_{1-89}$ protein complexes. Even more interesting, the spectra for the mixed metal species is superimposable with the Cd^{2+} spectra suggesting that Ca^{2+} has little impact on structure when Cd^{2+} is present.

4.5 Conclusions

The recent crystal structure from Zhang and coworkers [32] revealed seven Cd^{2+} ions binding to the protein. Our isothermal titration calorimetry data reveal that ~4 Cd^{2+} ions bind to the protein and that the other sites are too weak to be observed under our conditions. Our data also reveal that Cd^{2+} binds three orders of magnitude stronger than Ca^{2+}. Although ITC data do not indicate where these Cd^{2+} ions are bound, displacement studies reveal that the first Cd^{2+} binding to the protein is altered when Ca^{2+} ion is present. In addition, CD data indicate that Cd^{2+} ion changes the structure of $HcTnC_{1-89}$ albeit slightly, and that this structure predominates in the presence of Ca^{2+} ion. Previous studies from Chapter 3 suggest that a weaker Cd^{2+} ion binds to loop I in the context of the full length protein. We therefore conclude that the weaker Cd^{2+} ion also binds to loop I and that binding does not appear to be affected by the presence of Ca^{2+} in loop II. We also believe that the 4^{th} Cd^{2+} ion is perhaps is binding near loop I as observed in the

crystal structure due to the similarity of binding parameters but more studies need to be run in order to verify.

What was most interesting was the presence of two high affinity sites. The two high affinity sites in the full length protein were attributed to binding to the C-domain. This was also supported by precious NMR studies investigating Cd^{2+} binding to bovine cardiac troponin C. Furthermore, two additional high affinity sites were also not observed in the full length protein studies. The presence of Ca^{2+} binding to the $HcTnC_{1-89}$ appears to affect the mode of binding of the first high affinity Cd^{2+} ion. We propose that the two high affinity Cd^{2+} ions bind to the sulfur in Cys84 in a binuclear fashion as indicated in the crystal structure (Figure 9, Chapter 1). The absence of this thermodynamic signature in the full length protein may be due to the fact that Cys84 is very close to the linker region of the full length protein. Therefore, this cysteine residue may not be accessible to Cd^{2+} binding and is not observed in our full length binding studies. More studies are required to characterize these possible sites in $HcTnC_{1-89}$ and future studies may include mutant studies in combination with spectroscopic techniques such as Raman and ^{113}Cd NMR.

Chapter 5: Discussion and Future Directions

5.1. Further thermodynamic support for Cd^{2+} binding to EF I in cTnC

Although the crystal structure of N-cTnC was recently defined showing Cd^{2+} binding to the N terminal domain of cTnC there is no quantitative data that suggests Cd^{2+} is interacting at the EF I and EF II sites. Our studies provide the thermodynamic and structural analysis of Cd^{2+} interacting with full length and truncated HcTnC while Figure 9 in Chapter 1 demonstrates the possible sites in which Cd^{2+} binds to the N terminal site, as previously defined through the crystallized structure of Cd^{2+} bound cTnC. Analysis of our results, while using the crystalized representation of Cd^{2+} binding sites as a guide, we can gain a deeper insight as to where Cd^{2+} is binding to the protein.

In order to get a better idea of where Cd^{2+} is bound to the N domain of cTnC we first compared the thermodynamic data between the Ca^{2+} binding events from the full length and truncated studies in which only the Ca^{2+} binding site in the N terminal domain of CTnC was thought to be available. Based on our data we hypothesized, that Cd^{2+}, when titrated into apo cTnC, binds to the C terminal EF hand sites and a site other than EF II in the N domain of cTnC. Therefore, the first set of data included in Table 5 represents Ca^{2+} binding to Cd^{2+} bound HcTnC. In addition, the second row of values represents the third Ca^{2+} binding event to apo HcTnC while the last row demonstrates the thermodynamics associated with Ca^{2+} binding to truncated apo $HcTnC_{1\text{-}89}$. The thermodynamics and binding curves associated the data shown in second and third row of table 5 have been previously identified as Ca^{2+} binding to EF II loop in the N domain [132]. Based on similar ΔG for the three scenarios, it appears that loop II in N-domain is available for Ca^{2+} binding regardless of presence of Cd^{2+}. These similar values also

indicate that Ca^{2+} is not competing with Cd^{2+} for loop II, nor does Ca^{2+} appear to be competing for Cd^{2+} in the C-domain. Therefore, These data suggest that Cd^{2+} is binding to the protein at a site other than EF I, and interaction between Cd^{2+} and the protein does not interfere or compete with Ca^{2+} binding to the N domain of cTnC.

Table 6: Summary of Ca^{2+} Binding Data

Ca^{2+} Binding to…	ΔG kcal/mol	ΔH kcal/mol	TΔS kcal/mol
Apo HcTnC (n=3)	-6.4	1.3	7.7
Cd^{2+} bound HcTnC	-5.6	5	10.6
Apo $HcTnC_{1-89}$	-6.2	5.5	11.7

To supplement our conclusions, we also compared the thermodynamic data between the Cd^{2+} binding events from the full length and truncated studies in which the EF I site, or vestigial site, in the N terminal domain of cTnC was thought to be available.

The almost identical ΔG values as demonstrated in Table 7, suggests that the Cd^{2+} is binding to the same site in both full length and $HcTnC_{1-89}$, and appears to do so with the same ΔG regardless of the presence of Ca^{2+}. Also, the thermodynamics of Cd^{2+} binding to $HcTnC_{1-89}$ remain unchanged with or w/o Ca^{2+}present. Although previous Ca^{2+} data suggest that Cd^{2+} binds to loop II ,our data strongly demonstrates that Cd^{2+} is binding to EF I in the presence or absence of Ca^{2+}.

Table 7: Summary of Cd^{2+} Binding Data

Cd^{2+} Binding to…	ΔG kcal/mol	ΔH kcal/mol	TΔS kcal/mol
apo HcTnC (n=3)	-6.2	-1.3	4.9
Ca^{2+} bound HcTnC (n=3)	-6	-3.1	-2.9
apo $HcTnC_{1-89}$	-6.1	-9.5	-3.4
Ca^{2+} bound $HcTnC_{1-89}$	-6	-9.4	-3.4

To conclude, our results coupled to previous studies in the literature suggest that the putative binding sites for Cd^{2+} in cTnC, are the two C-domain sites and possibly the EF I site of cTnC in the full length protein. Additional sites in the isolated N-domain include a Cd^{2+} binding site near loop I or loop II and a binuclear site with bridging Cys84 residue located near the C-terminus (Figure 9a-c, Chapter 1). However, further studies are needed to verify these interactions.

5.2. Possible Effects of Cd^{2+} Binding to EF I on CVD

A recent study involving mutations of cTnC and the effects induced on Ca^{2+} infinity and the interaction occurring with cTnI [141]. In addition, further information on cardiac function was provided as a result of these effects. The preliminary results from the study demonstrated that ATPase activity increased due to prolonged contraction time as a result of a disruption in between the interaction of cTnI and cTnC [141]. These results thereby indicate that the interaction between cTnI and cTnC is critical for the heart muscle to efficiently transition from

contraction to relaxation phase. In addition, cTnI is regulated through PKA phosphorylation which phosphorylates the N extension of cTnI while bound to the N terminal cTnC. When this interaction was disabled there was a delay in phosphorylation of cTnI [141]. As a result ATPase activity increased, thereby indicating that the cardiac muscle protein units could have spent more time in the contracted state. Since our data indicates that Cd^{2+} is interfering with defunct loop I, and the amino acids speculated to bind Cd^{2+} at this site are also binding ligands for cTnI, additional ATPase studies involving Cd^{2+} cTnC and cTnI may produce similar results as the cTnC/ cTnI mutation study. If so then we could suspect that Cd^{2+} interacting with this pathway could potentially cause an increase in cardiac ATPase activity, thereby concluding that the interaction of Cd^{2+} at the EF I site in the N domain of cTnC is possible pathway metal toxicity leading to CVD disease.

Furthermore, other species have shown mutations in the EF I site that has also lead to changes in heart function. For example, ectothermic species have shown mutations ASn2, Ile28, Gln29, and Sp30 have functional importance in Ca^{2+} sensing at lower temperatures, such as having providing the TnC with a higher Ca^{2+} affinity [93]. How these mutations increase the affinity for Ca^{2+} is unknown. However, there is speculation that mutations in the N domain of cTnC may interfere with the interaction between cTnC and cTnI, which could have an effect on Ca^{2+} binding, and further effect the kinetics involved in cardiac muscle function as the heart transitions from the contracted to the relaxed state and vice versa. Although more data is needed to investigate evolutionary changes in cTnC and the effects of cTnI, the data available alludes to the conclusion that Cd^{2+} interaction at the N domain of cTnC, specifically in the EF I site, could impart serious implications on cardiac function.

5.3 Future Directions

In order to continue with our studies of Cd^{2+} binding to HcTnC and the implications on the function of the protein as a result of metal binding, we would need to investigate more specifically where Cd^{2+} binding is preferred in the N-domain of cTnC. Possible experiments to probe Cd^{2+} binding to loop I include ^{113}Cd NMR studies ,which display strong Cd^{2+} thiolate resonances at ~600 ppm, and Raman, which display Cd^{2+}-thiolate bond stretching frequencies. In addition, mutant studies involving both the C domain and N domain would further aid in pinpointing Cd^{2+} binding to the protein and also provide information on the interaction between the EF hand loops and N and C domains. Once Cd^{2+} ion binding regions have been identified, one can begin to probe the effect Cd^{2+} may have on cardiac muscle function and HcTnC's interactions with other troponin proteins. Cd^{2+} may be used to explore the novel cTnC and cTnI binding interactions.

References

[1] Williams RJP (2002) J Inorg Biochem 88:241-250.

[2] Krezel A, Hao Q, Maret W (2007) Arch Biochem Biophys 463:188-200.

[3] Irving H, Williams RJP (1948) Nature 162:746-747.

[4] Moulis J- (2010) Biometals 23:877-896.

[5] Canham-Rayner G, Overton T (2002) Descriptive Inorganic Chemistry. W.H. Freeman and Company, New York, NY.

[6] Maret W, Vallee BL (1998) Proc Natl Acad Sci USA 95:3478-3482.

[7] Maret W, Li Y (2009) Chem Rev 109:4682-4707.

[8] Michalska AE, Choo KHA (1993) Proc Natl Acad Sci USA 90:8088-8092.

[9] Zhao H, Farah A, Morel D, Ferekides CS (2009) Thin Solid Films 517:2365-2369.

[10] Gunter Buxbaum GP (2005). Wiley-VCH Verlag GmbH & Co. KGaA, Weinheim, Germany, pp 300 pgs.

[11] Miller LS, Mullin JB (1991). Plenum Press, New York,.

[12] Blindauer CA, Schmid R (2010) Metallomics 2:510-529.

[13] Krizek BA, Merkle DL, Berg JM (1993) Inorg Chem 32:937-940.

[14] Lane TW, Morel FMM (2000) Proc Natl Acad Sci U S A 97:4627-4631.

[15] Martin RB (1987) J Chem Educ 64:402.

[16] Misra RR, Hochadel JF, Smith GT, Cook JC, Waalkes MP, Wink DA (1996) Chem Res Toxicol 9:326-332.

[17] Cullen JT, Maldonado MT (2013) Metal Ions in Life Sciences 11:31-62.

[18] Satarug S, Baker JR, Urbenjapol S, Haswell-Elkins M, Reilly PEB, Williams DJ, Moore MR (2003) Toxicol Lett 137:65-83.

[19] Francesconi KA (2007) Analyst 132:17-20.

[20] McKenzie J, Kjellstrom T, Sharma R (1986) Cadmium Intake via Oysters and Health Effects in New Zealand: Cadmium Intake, Metabolism, and Effects in People with a High Intake of Ooysters in New Zealand.

[21] Copes R, Clark NA, Rideout K, Palaty J, Teschke K (2008) Environ Res 107:160-169.

[22] Haswell-Elkins M, Imray P, Satarug S, Moore MR, O'Dea K (2007) Journal of Exposure Science and Environmental Epidemiology 17:372-377.

[23] Satarug S, Moore MR (2004) Environ Health Perspect 112:1099-1103.

[24] Horiguchi H, Oguma E, Sasaki S, Miyamoto K, Ikeda Y, Machida M, Kayama F (2004) Toxicol Appl Pharmacol 196:114-123.

[25] Sahmoun AE, Case LD, Jackson SA, Schwartz GG, Schwartz GG (2005) Cancer Invest 23:256-263.

[26] Maret W, Moulis J- (2013) Metal Ions in Life Sciences 11:1-29.

[27] Dudley RE, Gammal LM, Klaassen CD (1985) Toxicol Appl Pharmacol 77:414-426.

[28] Limaye DA, Shaikh ZA (1999) Toxicol Appl Pharmacol 154:59-66.

[29] Everett CJ, Frithsen IL (2008) Environ Res 106:284-286.

[30] Åkesson A, Bjellerup P, Lundh T, Lidfeldt J, Nerbrand C, Samsioe G, Skerfving S, Vahter M (2006) Environ Health Perspect 114:830-834.

[31] Rosamond W, Flegal K, Friday G, Furie K, Go A, Greenlund K, Haase N, Ho M, Howard V, Kissela B, Kittner S, Lloyd-Jones D, McDermott M, Meigs J, Moy C, Nichol G, O'Donnell CJ, Roger V, Rumsfeld J, Sorlie P, Steinberger J, Thom T, Wasserthiel-Smoller S, Hong Y (2007) Circulation 115:e69-e171.

[32] Zhang XL, Tibbits GF, Paetzel M (2013) Acta Crystallographica Section D: Biological Crystallography 69:722-734.

[33] Li AY, Lee J, Borek D, Otwinowski Z, Tibbits GF, Paetzel M (2011) J Mol Biol 413:699-711.

[34] Leavis PC, Kraft EL (1978) Arch Biochem Biophys 186:411-415.

[35] Farah CS, Reinach FC (1995) FASEB Journal 9:755-767.

[36] Freisinger E, Vašák M (2013) Metal Ions in Life Sciences 11:339-371.

[37] Langmade SJ, Ravindra R, Daniels PJ, Andrews GK (2000) J Biol Chem 275:34803-34809.

[38] Troadec M-, Ward DM, Lo E, Kaplan J, De Domenico I (2010) Blood 116:4657-4664.

[39] Carvalho E, Gothe PO, Bauer R, Danielsen E, Hemmingsen L (1995) European Journal of Biochemistry 234:780-785.

[40] Margoshes M (1957) J Am Chem Soc 79:4813-4814.

[41] Méplan C, Mann K, Hainaut P (1999) J Biol Chem 274:31663-31670.

[42] Clarkson TW (1993) Annu Rev Pharmacol Toxicol 33:545-571.

[43] Ohana E, Sekler I, Kaisman T, Kahn N, Cove J, Silverman WF, Amsterdam A, Hershfinkel M (2006) Journal of Molecular Medicine 84:753-763.

[44] Maret W (2006) Antioxidants and Redox Signaling 8:1419-1441.

[45] Kjellstrom T (1979) Environ Health Perspect Vol. 28:169-197.

[46] Nordberg GF, Kjellstrom T (1979) Environ Health Perspect Vol. 28:211-217.

[47] Tsuchiya K, Sugita M, Seki Y (1976) Keio J Med 25:73-82.

[48] Jalilehvand F, Leung BO, Mah V (2009) Inorg Chem 48:5758-5771.

[49] Meijers R, Morris RJ, Adolph HW, Merli A, Lamzin VS, Cedergren-Zeppezauer ES (2001) J Biol Chem 276:9316-9321.

[50] Xu Y, Feng L, Jeffrey PD, Shi Y, Morel FMM (2008) Nature 452:56-61.

[51] Lane TW, Saito MA, George GN, Pickering IJ, Prince RC, Morell FMM (2005) Nature 435:42.

[52] Friedman R (2014) Dalton Trans 43:2878-2887.

[53] Jacobson KB, Turner JE (1980) Toxicology 16:1-37.

[54] Choong G, Liu Y, Templeton DM (2014) Chem Biol Interact 211:54-65.

[55] Clarke TE, Vogel HJ (2002) Methods Mol Biol 173:205-215.

[56] Ellis PD, Strang P, Potter JD (1984) J Biol Chem 259:10348-10356.

[57] Rao ST, Satyshur KA, Greaser ML, Sundaralingam M (1996) Acta Crystallographica Section D: Biological Crystallography 52:916-922.

[58] Forsen S, Linse S (1995) Trends Biochem Sci 20:495-497.

[59] Andersson A, Forsen S, Thulin E, Vogel HJ (1983) Biochemistry 22:2309-2313.

[60] Swain AL, Amma EL (1989) Inorg Chim Acta 163:5-7.

[61] Leinala EK, Arthur JSC, Grochulski P, Davies PL, Elce JS, Jia Z (2003) Proteins: Structure, Function and Genetics 53:649-655.

[62] Chao SH, Suzuki Y, Zysk JR, Cheung WY (1984) Mol Pharmacol 26:75-82.

[63] Langer GA, Nudd LM (1983) Circ Res 53:482-490.

[64] Bertini I, Gray BH, Stiefel IE, Valentine SJ (2007) Biological Inorganic Chemistry; Structure and Reactivity. University Science Books, Sausalito, California.

[65] Gifford JL, Walsh MP, Vogel HJ (2007) Biochem J 405:199-221.

[66] Ikura M (1996) Trends Biochem Sci 21:14-17.

[67] Henikoff S, Greene EA, Pietrokovski S, Bork P, Attwood TK, Hood L (1997) Science 278:609-614.

[68] Nelson MR, Chazin WJ (1998) Biometals 11:297-318.

[69] Berg J, Tymoczko J, Stryer L (2007) Biochemistry. 6th Ed. W.H. Freeman and Company, New York, New York.

[70] Nelson MR, Thulin E, Fagan PA, Forsén S, Chazin WJ (2002) Protein Science 11:198-205.

[71] Finn BE, Evenas J, Drakenberg T, Waltho JP, Thulin E, Forsen S (1995) Nat Struct Biol 2:777-783.

[72] Kuboniwa H, Tjandra N, Grzesiek S, Ren H, Klee CB, Bax A (1995) Nat Struct Biol 2:768-776.

[73] Zhang M, Tanaka T, Ikura M (1995) Nat Struct Biol 2:758-767.

[74] Skelton NJ, Kördel J, Akke M, Forsén S, Chazin WJ (1994) Nat Struct Biol 1:239-245.

[75] McPhalen CA, Strynadka NC, James MN (1991) Adv Protein Chem 42:77-144.

[76] Evenas J, Malmendal A, Akke M (2001) Structure 9:185-195.

[77] Strynadka NC, Cherney M, Sielecki AR, Li MX, Smillie LB, James MN (1997) J Mol Biol 273:238-255.

[78] Li MX, Gagne SM, Tsuda S, Kay CM, Smillie LB, Sykes BD (1995) Biochemistry 34:8330-8340.

[79] Gagné SM, Tsuda S, Li MX, Smillie LB, Sykes BD (1995) Nat Struct Biol 2:784-789.

[80] Godzik A, Sander C (1989) Protein Eng 2:589-596.

[81] Babu YS, Sack JS, Greenhough TJ, Bugg CE, Means AR, Cook WJ (1985) Nature 315:37-40.

[82] Herzberg O, James MNG (1988) J Mol Biol 203:761-779.

[83] Kretsinger RH, Rudnick SE, Weissman LJ (1986) J Inorg Biochem 28:289-302.

[84] Krebs J, Heizmann CW In: Krebs J, Michalak M (eds), New Comprehensive Biochemistry. Elsevier pp 51-93.

[85] Spyracopoulos L, Li MX, Sia SK, Gagne SM, Chandra M, Solaro RJ, Sykes BD (1997) Biochemistry 36:12138-12146.

[86] Li MX, Spyracopoulos L, Sykes BD (1999) Biochemistry 38:8289-8298.

[87] Belmont LD, Orlova A, Drubin DG, Egelman EH (1999) Proc Natl Acad Sci U S A 96:29-34.

[88] Chalovich JM, Chock PB, Eisenberg E (1981) J Biol Chem 256:575-578.

[89] Chalovich JM, Eisenberg E (1982) J Biol Chem 257:2432-2437.

[90] Gordon AM, Homsher E, Regnier M (2000) Physiol Rev 80:853-924.

[91] Ebashi S, Endo M, Otsuki I (1969) Q Rev Biophys 2:351-384.

[92] Franklin A, Baxley T, Kobayashi T, Chalovich J (2012) Biophys J 102:2536-2544.

[93] Gillis TE, Marshall CR, Tibbits GF (2007) Physiological Genomics 32:16-27.

[94] Chao S, Bu C, Cheung WY (1990).

[95] van Eerd J, Takahashi K (1975) Biochem Biophys Res Commun 64:122-127.

[96] Takahashi K (1976) Biochemistry 15:1171-1180.

[97] Li MX, Gagne SM, Spyracopoulos L, Kloks CPAM, Audette G, Chandra M, Solaro RJ, Smillie LB, Sykes BD (1997) Biochemistry 36:12519-12525.

[98] Shaw GS, Sykes BD, Marsden BJ (1990) Biochemistry and Cell Biology 68:587-601.

[99] Collins JH (1997) Biochemistry 30:702-707.

[100] Sia SK, Li MX, Spyracopoulos L, Gagne SM, Liu W, Putkey JA, Sykes BD (1997) J Biol Chem 272:18216-18221.

[101] Sadayappan S, Finley N, Howarth JW, Osinska H, Klevitsky R, Lorenz JN, Rosevear PR, Robbins J (2008) FASEB Journal 22:1246-1257.

[102] Howarth JW, Meller J, Solaro RJ, Trewhella J, Rosevear PR (2007) J Mol Biol:373,-706–722.

[103] Mittmann K, Jaquet K, Heilmeyer Jr. LMG (1990) FEBS Lett 273:41-45.

[104] Solaro RJ, Moir AJG, Perry SV (1976) Nature 262:615-617.

[105] Sakthivel S, Finley NL, Rosevear PR, Lorenz JN, Gulick J, Kim S, VanBuren P, Martin LA, Robbins J (2005) J Biol Chem 280:703-714.

[106] Ray KP, England PJ (1976) FEBS Lett 70:11-16.

[107] Mittmann K, Jaquet K, Heilmeyer Jr. LMG (1992) FEBS Lett 302:133-137.

[108] Haworth RS, Cuello F, Herron TJ, Franzen G, Kentish JC, Gautel M, Avkiran M (2004) Circ Res 95:1091-1099.

[109] Robertson SP, Johnson JD, Holroyde MJ, Kranias EG, Potter JD, Solaro RJ (1982) J Biol Chem 257:260-263.

[110] Zhang R, Zhao J, Potter JD (1995) J Biol Chem 270:30773-30780.

[111] Reiffert SU, Jaquet K, Heilmeyer Jr. LMG, Ritchie MD, Geeves MA (1996) FEBS Lett 384:43-47.

[112] Kentish JC, McCloskey DT, Layland J, Palmer S, Leiden JM, Martin AF, Solaro RJ (2001) Circ Res 88:1059-1065.

[113] Abbott MB, Dong W-, Dvoretsky A, DaGue B, Caprioli RM, Cheung HC, Rosevear PR (2001) Biochemistry 40:5992-6001.

[114] Abbott MB, Dvoretsky A, Gaponenko V, Rosevear PR (2000) FEBS Letters 469:168-172.

[115] Finley N, Abbott MB, Abusamhadneh E, Gaponenko V, Dong W-, Gasmi-Seabrook G, Howarth JW, Rance M, Solaro RJ, Cheung HC, Rosevear PR (1999) FEBS Lett 453:107-112.

[116] Gaponenko V, Abusamhadneh E, Abbott MB, Finley N, Gasmi-Seabrook G, Solaro RJ, Rance M, Rosevear PR (1999) J Biol Chem 274:16681-16684.

[117] Ferrières G, Pugnière M, Mani J-, Villard S, Laprade M, Doutre P, Pau B, Granier C (2000) FEBS Lett 479:99-105.

[118] Ward DG, Brewer SM, Gallon CE, Gao Y, Levine BA, Trayer IP (2004) Biochemistry 43:5772-5781.

[119] Richardt G, Federolf G, Habermann E (1986) Biochem Pharmacol 35:1331-1335.

[120] Robertson IM, Sun Y-, Li MX, Sykes BD (2010) J Mol Cell Cardiol 49:1031-1041.

[121] Wang X, Li MX, Sykes BD (2002) J Biol Chem 277:31124-31133.

[122] Huang K-, Chiou S-, Ko T-, Yuann J-, Wang AH- (2002) Acta Crystallographica Section D: Biological Crystallography 58:1118-1128.

[123] Benning MM, Shim H, Raushel FM, Holden HM (2001) Biochemistry 40:2712-2722.

[124] Ferraroni M, Rypniewski W, Wilson KS, Viezzoli MS, Banci L, Bertini I, Mangani S (1999) J Mol Biol 288:413-426.

[125] Adiele RC, Stevens D, Kamunde C (2012) Toxicology in Vitro 26:164-173.

[126] Mastrángelo M, Dos Santos Afonso M, Ferrari L (2011) Ecotoxicology 20:1225-1232.

[127] Kometani K, Yamada K (1983) Biochem Biophys Res Commun 114:162-167.

[128] Grossoehme NE, Spuches AM, Wilcox DE (2010) J Biol Inorg Chem 15:1183-1191.

[129] Freyer MW, Lewis EA (2008) Biophysical Tools for Biologists: Vol 1 in Vitro Techniques 84:79-113.

[130] ITC Data Analysis in Origin (January 2004).

[131] Homans SW (2007) Bioactive Conformation i 272:51-82.

[132] Skowronsky RA, Schroeter M, Baxley T, Li Y, Chalovich JM, Spuches AM (2013) Journal of Biological Inorganic Chemistry 18:49-58.

[133] Kelly SM, Price NC (2000) Current Protein and Peptide Science 1:349-384.

[134] Johnson WC, Jr. (1990) Proteins: Structure, Function, and Bioinformatics 7:205–214.

[135] Rodger A, Nordén B (1997) Circular Dichroism and Linear Dichroism. Oxford University Press, Oxford.

[136] Magyar JS, Godwin HA (2003) Anal Biochem 320:39-54.

[137] Sia SK, Li MX, Spyracopoulos L, Gagne SM, Putkey JA, Sykes BD (1997) Biophys J 72:WP191-WP191.

[138] Potter JD, Hsu FJ, Pownall HJ (1977) J Biol Chem 252:2452-2454.

[139] Li MX, Chandra M, Pearlstone JR, Racher KI, Trigogonzalez G, Borgford T, Kay CM, Smillie LB (1994) Biochemistry 33:917-925.

[140] Teleman O, Drakenberg T, Forsen S, Thulin E (1983) Eur J Biochem 134:453-457.

[141] Schmidtmann A, Lindow C, Villard S, Heuser A, Mugge A, Gebner R, Granier C, Jaquet K (2005) FEBS:6087-6097.

Appendix A. Purification of HcTnC1-89 and Full length HcTnC

PET3d plasmid vectors containing genes coding for HcTnC and $HcTnC_{1-89}$ were generously donated by the Chalovich Lab at the Brody School of Medicine and were isolated and purified according to the protocol designed for the QlAprep spin Miniprep Kit. These plasmids were further transformed into cell lines XL1 Blue and BL21(DE3)pLysS respectively and stored at -80 °C until further use.

Full length HcTnC and HcTnC (1-89) were overexpressed in their appropriate cell lines and purified using separate methods. The procedure used for protein expression and purification of full length HcTnC is described first, followed by the methods used to grow and isolate $HcTnC_{1-89}$.

A.1 Expression and Purification of Full Length HcTnC

Cell stock's containing the transformed XL1 Blue bacterial cells were removed from the -80 °C freezer and streaked on to an LB agar plate containing 100 μg/mL of ampicillin. This medium was incubated at 37 °C overnight. The following day a single colony was removed and transferred into a 400 mL solution of LB broth containing 100 μg/mL of ampicillin. To achieve over-expressed protein levels, this 400 mL starter culture was allowed to grown shake overnight at 37 °C and 225 RPM. The next day 100 mL's of this culture were transferred into four separate Fernbach flasks each containing a 900 mL solution of LB broth and 100 μg/mL of ampicillin. The four 1L cultures were allowed to shake at 37 °C and 225 RPM until the optical density of the solution measured at 600 nm reached an absorbance of 1.5. Once achieved, the cultured solutions

were centrifuged for 15 minutes at 4°C at 4000 RPM. The resulting supernatant was discarded and the remaining pellet was prepared for purification.

Following centrifugation of the culture, the resulting pellet was resuspended in a buffer solution containing 1 mM ethylenediaminetetraacetic acid (EDTA), 50 mM Tris/HCl (pH=8.0) at about 10-15 mL of resuspension buffer per liter of culture. A second solution containing 43 mg of protease cocktail in 0.2 mL of DMSO/0.8 mL of 18Ω water and 20 mg of deoxycholate was brought to 4 mL with 18Ω water was added to the resuspended pellet. The solution was mixed thoroughly on ice until the pellet was completely resuspended. Approximately 50 mL of the resuspended solution was transferred to a clean sonication tube. This solution was then placed on ice and allowed to stir while sonicating at 2 min intervals set at a 30 seconds on 30 seconds off pulse rate (40% amplitude).

The lysed samples were combined, mixed, and then centrifuged at 18,000 RPM for 15 mins at 4°C. The supernatant was collected and the total volume was recorded. This value was then used to calculate the grams of salt needed to bring the solution to a final concentration of 5 mM $CaCl_2$ and 1 mM $MgCl_2$. Ammonium sulfate was then added to produce 60% saturation. The sample was mixed and then centrifuged for 20 minutes at 18,000 RPM and 4°C. The resulting supernatant was collected and purified using a phenyl sepharose CL-4B column via hydrophobic chromatography.

The supernatant was added to a 30 mL phenyl sepharose CL-4B column that had been pre-equilibrated using 500 mL of a buffer containing 1 M NaCl, 1 mM $CaCl_2$ and 50 mM Tris/HCl at a pH=8.0. The sample was washed with 500 mL of the equilibration buffer. Then, a solution gradient was set up to wash the sample with 300-500 mL of wash buffer followed by 300- 500 mL of elution buffer. Wash buffer contained 1 M NaCl, 0.2 mM $CaCl_2$ and 50 mM

Tris/HCl at a pH=8.0 while elution buffer consisted of 5 mM EDTA and 20 mM Tris/HCl pH=8.0.

A gravity flow system was used to elute samples from the column. These samples were collected in 5 mL increments using the Retriever Fraction Collector. The absorbance of each fraction was measured and recorded using UV-vis spectroscopy (Thermo Scientific NanoDrop 2000C spectrophotometer) at 280 nm. Fractions producing a large absorbances, specifically those eluted in elution buffer, were tested for impurities via gel electrophoresis using a 12% polyacrylamide gel (Figure A1).

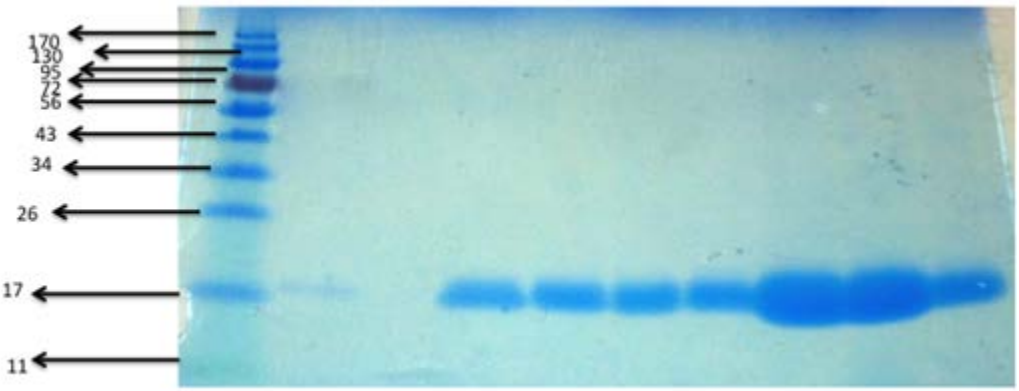

Figure A1. A 12% polyacrylamide Gel showing fractions eluted with 5mM EDTA 20mM Tris/HCl. Gel represents fractions contained pure HcTnC. The molecular marker (in kDa) used was an EZ-Run^{TM} Pre-stained Rec Protein Ladder shown in lane 1.

Fractions demonstrating little to no impurities were collected and either stored in -80 °C or used immediately in experimental analysis. Beer's law was then used to calculate the Protein concentrations for these samples using an extinction coefficient (Є) of 4595 cm^{-1} M^{-1}, a path

length of 1 cm and the absorbance value for that sample in a Beer's Law calculation. This value was recorded and used in calculations involved in the experimental design.

A.2 Expression and Purification of $HcTnC_{1-89}$

Cell stock's containing the transformed BL21(DE3)pLysS bacterial cells were removed from the -80 °C freezer and streaked on to an LB agar plate containing 100 μg/mL of ampicillin. This medium was incubated at 37 °C overnight. The following day a sterile batch of 400 mL of LB broth containing 100 μg/mL ampicillin was inoculated with a colony produced on the agar plate. This starter culture was incubated overnight at 37 °C at 225 RPM.

The following morning four Fernbach flasks, each containing a sterilized solution of 900 mL of LB broth and 100 μg/mL of ampicillin, were prepared. To each Fernbach flask, 100 mL of the O/N culture was added. After an hour of growth at 37°C and 225 RPM, the optical density of the solution was measured at 600 nm. If the solution did not obtain an optical density between 0.8-1.000 in the first measurement, incubation was continued while performing frequent measurements.

When the optical density of the solution rose to the optimal range, protein expression was then induced by adding stock solutions solution of isopropyl β-D-thiogalactopyranoside to a final concentration of 5 mM. The cells were allowed to incubate at 37 °C and 225 RPM for 4 hours. Following this time, the solution was centrifuged at 4000 RPM in 15 minute intervals. The supernatant was discarded and the pellet was resuspended and purified. For a more successfully purification of $HcTnC_{1-89}$, half of the resulting pellet was used while the other half was stored at -80 °C until further purified.

The cell pellet of the cultured solution was resuspended by adding a 5 mL lysozyme solution for every liter of culture. The lysozyme solution consisted of 1mg/ml of lysozyme in 20% sucrose, 20 mM Tris-HCl at pH 7.5, 1 mM EDTA, and 0.2 mM phenylmethylsulfonyl fluoride. After incubating the resuspended solution at 4 °C for 20 minutes, 20 mL (per liter of cell culture) was added of the following solution: of 20 mM Tris-HCl at pH7.5, 1 mM EDTA, 0.5 mM dithiothreitol and 0.2 mM phenylmethylsulfonyl fluoride. The solution was then stirred on ice at 4 °C for 10-15 minutes and then sonicated for 4 mins at a 25% duty cycle, and an output control of 2.5. The sample was then centrifuged at 18000 RPM for 15 minutes at 4 °C.

The supernatant was collected fixed to a final concentration of 10mM $CaCl_2$, 1 M NaCl and then slowly added onto on a 100 mL phenyl-Sepharose CL-4B column at room temperature via gravity flow. Runoff was collected in 5 mL samples. Prior to adding the sample to the column, the column had been equilibrated with 500 mL wash buffer I consisting of 50 mM Tris-HCl at pH 7.5, 10 mM $CaCl_2$, 1 mM $MgCl_2$, 1 mM DTT and 1 M NaCl.

Once the sample was loaded onto the column 300 mL of wash buffer I was then used to wash the sample. Wash buffer II consisting of 50 mM Tris-HCl at pH 7.5, 5 mM $CaCl_2$, 1 M NaCl, and 1 mM DTT and wash buffer 3 consisting of 50 mM Tris-HCl at pH 7.5, 0.1 mM $CaCl_2$, 1 M NaCl, and 1 mM DTT were washed over the sample in a gradient fashion. An elution buffer of 50 mM Tris-HCl at pH 7.5, 1 mM EDTA, and 1 mM DTT was then used to elute the protein from the column. 5 mL fractions were collected during all washes and elution. The absorbances of each fraction were measured. The purity of fractions giving large absorbance values was tested using gel electrophoresis (Figure A2). The molecular weight of HcTnC is approximately 10 kD.

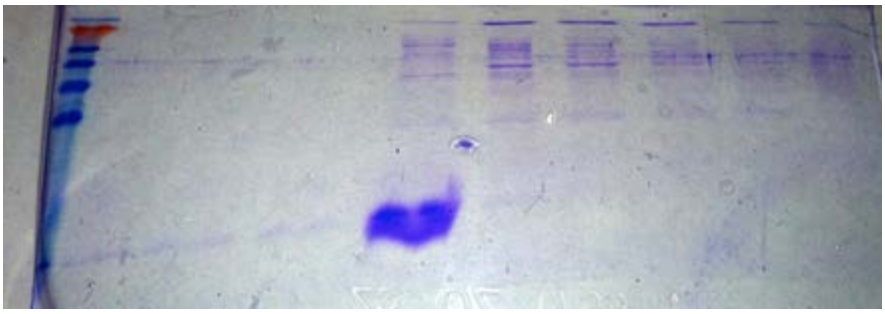

Figure A2. A 15% polyacrylamide Gel showing fractions eluted with 50 mM Tris-HCl at pH 7.5, 1 mM EDTA, and 1 mM DTT. Gel represents fractions containing slightly pure HcTnC(1-89). The molecular marker used was a "Prestained Rec Protein Ladder" shown in lane 1.

In order to ensure that all protein was Ca^{2+} free the protein was brought to 2 mM EDTA concentration. The protein was then dialyzed against the buffer to be used in ITC experiments. The buffers used was 50 mM Bis-Tris pH 7.0, 50 mM KCl. The dialysis was performed with 1 liter of the dialysis buffer three times with four hours between each liter. All buffer solutions were adjusted to a pH=7.0.

Calcium and cadmium stock solutions of 5 mM were prepared in each buffer. The metal and protein solutions to be used in ITC experiments were diluted with the corresponding dialysis buffer. Preparation of Ca^{2+} solutions in this manner served to ensure that protein and metal were in identical buffer.